N O T I C E

THIS DOCUMENT HAS BEEN REPRODUCED FROM MICROFICHE. ALTHOUGH IT IS RECOGNIZED THAT CERTAIN PORTIONS ARE ILLEGIBLE, IT IS BEING RELEASED IN THE INTEREST OF MAKING AVAILABLE AS MUCH INFORMATION AS POSSIBLE

NAVAL POSTGRADUATE SCHOOL
Monterey, California

THESIS

AN AERODYNAMIC PERFORMANCE EVALUATION
OF THE NASA/AMES RESEARCH CENTER
ADVANCED CONCEPTS FLIGHT SIMULATOR

by

Paul F. Donohue

June 1987

Thesis Advisor: Chester A. Heard

87   9 25 074

'2A18 4 700

REPORT DOCUMENTATION PAGE

1a REPORT SECURITY CLASSIFICATION UNCLASSIFIED	1b RESTRICTIVE MARKINGS			
2a SECURITY CLASSIFICATION AUTHORITY	3 DISTRIBUTION/AVAILABILITY OF REPORT Approved for public release; distribution is unlimited			
2b DECLASSIFICATION / DOWNGRADING SCHEDULE				
4 PERFORMING ORGANIZATION REPORT NUMBER(S)	5 MONITORING ORGANIZATION REPORT NUMBER(S)			

6a NAME OF PERFORMING ORGANIZATION Naval Postgraduate School	6b OFFICE SYMBOL (If applicable) Code 67	7a NAME OF MONITORING ORGANIZATION Naval Postgraduate School
6c ADDRESS (City, State, and ZIP Code) Monterey, California 93943-5000		7b ADDRESS (City, State, and ZIP Code) Monterey, California 93943-5000
8a NAME OF FUNDING/SPONSORING ORGANIZATION	8b OFFICE SYMBOL (If applicable)	9 PROCUREMENT INSTRUMENT IDENTIFICATION NUMBER

8c ADDRESS (City, State, and ZIP Code)	10 SOURCE OF FUNDING NUMBERS			
	PROGRAM ELEMENT NO	PROJECT NO	TASK NO	WORK UNIT ACCESSION NO

11 TITLE (Include Security Classification)
AN AERODYNAMIC PERFORMANCE EVALUATION OF THE NASA/AMES RESEARCH CENTER
ADVANCED CONCEPTS FLIGHT SIMULATOR

12 PERSONAL AUTHOR(S)
Donohue, Paul F.

13a TYPE OF REPORT Master's Thesis	13b TIME COVERED FROM _____ TO _____	14 DATE OF REPORT (Year, Month, Day) 1987, June	15 PAGE COUNT 113

16 SUPPLEMENTARY NOTATION

17	COSATI CODES		18 SUBJECT TERMS (Continue on reverse if necessary and identify by block number)
FIELD	GROUP	SUB-GROUP	Aircraft Simulation; Transport Aircraft
			Simulation; Aircraft Performance; Performance
			Test Techniques

19 ABSTRACT (Continue on reverse if necessary and identify by block number)

The results of an aerodynamic performance evaluation of the National Aeronautics and Space Administration (NASA)/Ames Research Center Advanced Concepts Flight Simulator (ACFS), conducted in association with the Navy-NASA Joint Institute of Aeronautics, are presented. The ACFS is a full-mission flight simulator which provides an excellent platform for the critical evaluation of emerging flight systems and aircrew performance. The propulsion and flight dynamics models were evaluated using classical flight test techniques. The aerodynamic performance model of the ACFS was found to realistically represent that of current day, medium range transport aircraft. Recommendations are provided to enhance the capabilities of the ACFS to a level forecast for 1995 transport aircraft. The

20 DISTRIBUTION/AVAILABILITY OF ABSTRACT ☒ UNCLASSIFIED/UNLIMITED ☐ SAME AS RPT ☐ DTIC USERS	21 ABSTRACT SECURITY CLASSIFICATION Unclassified	
22a NAME OF RESPONSIBLE INDIVIDUAL LCDR C.A. Heard USN	22b TELEPHONE (Include Area Code) (408) 646-2716	22c OFFICE SYMBOL Code 67Ha

DD FORM 1473, 84 MAR 83 APR edition may be used until exhausted
All other editions are obsolete

SECURITY CLASSIFICATION OF THIS PAGE
UNCLASSIFIED

1

#19 - ABSTRACT - (CONTINUED)

graphical and tabular results of this study will
establish a performance section of the ACFS
Operation's Manual.

Accession For

NTIS GRA&I
DTIC TAB
Unannounced
Justification

By
Distribution/
Availability Codes
Dist | Avail and/or
| Special

A-1

QUALITY
INSPECTED
2

An Aerodynamic Performance Evaluation
of the NASA/Ames Research Center
Advanced Concepts Flight Simulator

by

Paul F. Donohue
Major, United States Marine Corps
B.S., United States Naval Academy, 1972
M.B.A., Texas A&I University, 1981

Submitted in partial fulfillment of the
requirements for the degree of

MASTER OF SCIENCE IN AERONAUTICAL ENGINEERING
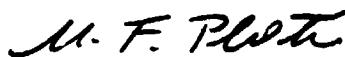
from the

NAVAL POSTGRADUATE SCHOOL
June 1987

Author: _____
Paul F. Donohue

Approved by: _____
Chester A. Heard, Thesis Advisor

_____
M.F. Platzer, Chairman
Department of Aeronautics

_____
G.E. Schacher
Dean of Science and Engineering

3

ABSTRACT

The results of an aerodynamic performance evaluation of the National Aeronautics and Space Administration (NASA)/Ames Research Center Advanced Concepts Flight Simulator (ACFS), conducted in association with the Navy-NASA Joint Institute of Aeronautics, are presented. The ACFS is a full-mission flight simulator which provides an excellent platform for the critical evaluation of emerging flight systems and aircrew performance. The propulsion and flight dynamics models were evaluated using classical flight test techniques. The aerodynamic performance model of the ACFS was found to realistically represent that of current day, medium range transport aircraft. Recommendations are provided to enhance the capabilities of the ACFS to a level forecast for 1995 transport aircraft. The graphical and tabular results of this study will establish a performance section of the ACFS Operation's Manual.

TABLE OF CONTENTS

LIST OF FIGURES

8

LIST OF SYMBOLS

a	Acceleration
ACFS	Advanced Concepts Flight Simulator
AOA	Angle of attack
ATC	Air Traffic Control
C_D	Coefficient of drag
C_L	Coefficient of lift
$C_{L\ max}$	Maximum coefficient of lift
E_h	Energy height
EPR	Engine pressure ratio
F	Force
F_a	Force of acceleration
FAA	Federal Aviation Administration
F_f	Force of friction
ft	Feet
g	Gravitational constant
h	Altitude
KE	Kinetic energy
KIAS	Knots indicated airspeed
KTAS	Knots true airspeed
L	Lift
lbs	Pounds
M	Mach number
max	Maximum

mi	Miles
min	Minimum
NASA	National Aeronautics and Space Administration
PE	Potential energy
P_s	Specific excess power
rad	Radians
ROC	Rate of Climb
RPM	Revolutions per minute
S	Wing area
s	Distance
S_g	Ground distance
sec	Seconds
T	Thrust
t	Time
TE	Total energy
T/O	Take-off
TSFC	Thrust specific fuel consumption
V	Velocity
V_{app}	Approach speed
V_{lnd}	Landing speed
V_{lof}, V_2	Lift-off speed
V_r	Rotation speed
V_s	Stall speed
W	Weight
α	Thrust lapse rate
ρ	Density

σ	Density ratio
ϕ	Runway inclination angle
μ	Coefficient of friction
θ	Pitch angle
δ	Pressure ratio

ACKNOWLEDGMENTS

I am grateful to the following individuals for the support and assistance they provided:

- Mr. Bob Shiner, Director, Man-Vehicle Systems Research Facility, NASA/Ames Research Center

- LTCOL T.R. White USMCR, former Director of Research, Singer-Link, MVSRF, NASA/Ames Research Center

- LCDR Chet Heard USN, Thesis Advisor, Naval Postgraduate School

- Professor Rick Howard, Naval Postgraduate School.

I. INTRODUCTION

A. BACKGROUND

The design of current aircraft flight stations has
evolved through the incorporation of improved or modernized
controls and displays for individual systems. In most
instances, new displays and controls have simply replaced
outmoded units. This ad hoc process has not only produced a
conglomeration of knobs, switches, and displays but has also
frequently resulted in high crew workload, missed signals,
and misinterpreted information. Recent advances in flight
station design, however, indicate that improved display and
control systems will provide for safer and more efficient
system operation through a reduction in clutter, and a more
orderly and logical control of information to the flight
crew.

The Federal Aviation Administration (FAA) estimates that
nationwide flight operations will nearly double by the year
2000 [Ref. 1]. Several systems currently under development
dealing with this increase in air traffic include
conflict-alert/conflict-advisory systems, traffic alert and
collision avoidance systems, automated enroute air traffic
control systems, and improved communication and navigation
systems. Each of these systems will have a major impact on
aircraft and aircrew operating procedures, yet only a few

will immediately replace an existing system. Because of the dramatic advances in electronic and computer technology, it is imperative to assess the impact of new systems on crew performance in order to optimize the flight station design.

The Advanced Concepts Flight Simulator (ACFS) is a full-mission flight simulator which incorporates the real world factors that a flight crew would encounter on an operational mission, and, as such, is an excellent research, development, and testing device. A very realistic environment can be provided for aircrew to check the feasibility and acceptability of emerging crew systems before the expensive, detailed design process for that aircraft occurs.

This report presents the results of an aerodynamic performance evaluation of the National Aeronautics and Space Administration (NASA)/Ames Research Center Advanced Concepts Flight Simulator, conducted in Association with the Navy-NASA Joint Institute of Aeronautics. The ACFS is part of the Man-Vehicle Systems Research Facility at NASA/Ames. The propulsion and flight dynamics models were evaluated using classical flight test techniques as described in the body of this report. It is intended that the graphical and tabular results of this report be used to establish a performance section of the ACFS Operations Manual.

The performance evaluation was conducted over a four month period ending in April 1987. Over forty hours of

simulated flight time were accumulated in the course of this evaluation.

B. GENERAL DESCRIPTION OF ACFS

The Advanced Concepts Flight Simulator is designed to simulate a wide-body, T-tail, low wing transport aircraft with twin turbofan engines and a crew of two (Figure 1). It was formulated and sized based upon projected user needs for the year 1995 and a forecasted technology cutoff date of 1990 [Ref. 1]. The aircraft has a maximum gross take-off weight of approximately 224,000 pounds, carries a payload of 60,000 pounds, and can accommodate up to 200 passengers.

The aircraft has a conventional planform, high aspect ratio, supercritical wing. The flight control system utilizes conventional flight surfaces with stability augmentation provided in all three axes. All flight control surfaces are powered by electrical actuators and controlled by a digital fly-by-wire/light system. Manual flight control is accomplished through side stick controllers, which provide rate commands to the control system. This system replaces the conventional yoke system used in most current aircraft.

The cockpit is configured in a desk-top arrangement, with control display units and keyboards in front of each pilot, a side stick controller outboard of each pilot on the desk-top, and five cathode ray tubes for the interchangeable

41.67 FT.

161.25 FT.

139.67 FT.
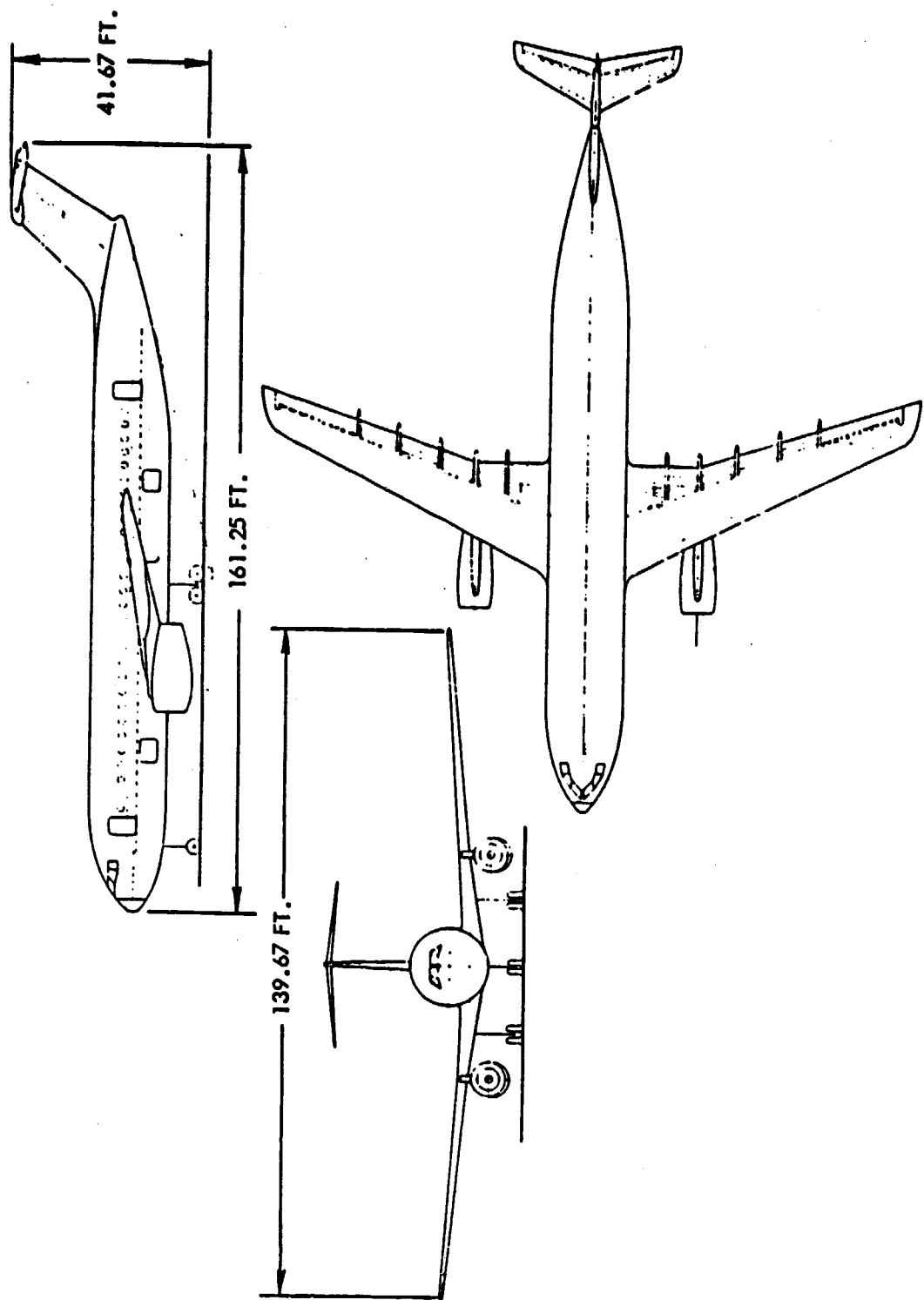
Figure 1. Generic Aircraft Layout

16

display of flight, navigation, and aircraft systems information (Figure 2).

The ACFS is designed to operate at one of five selectable take-off gross weights, from 150,000 to 220,000 pounds. Each gross weight selection has a preset onboard fuel and payload weight that is normally not altered. A complete listing of ACFS design characteristics is contained in Appendix A.

C. PRE-TEST PREPARATIONS

As an aid to data reduction, several lines of computer code were inserted into the ACFS flight dynamics module, a FORTRAN program which executes the aircraft six degree-of-freedom equations of motion. The program uses forces and torques from the aerodynamics, ground dynamics, and propulsion programs, as well as weight, inertia, and environmental data to calculate the aircraft position, attitude, rates, and accelerations. The additional code provides the advantages of both standardizing the overall data reduction process and eliminating the need for most hand calculations outside the program. Appendix B contains the additional lines of code and definitions of each variable used in the code.

A debug page containing twenty variables was constructed in order to allow for easy access to the model variables (Figure 3). Prior to each test run, the debug page was called up and displayed on a computer screen in the aft
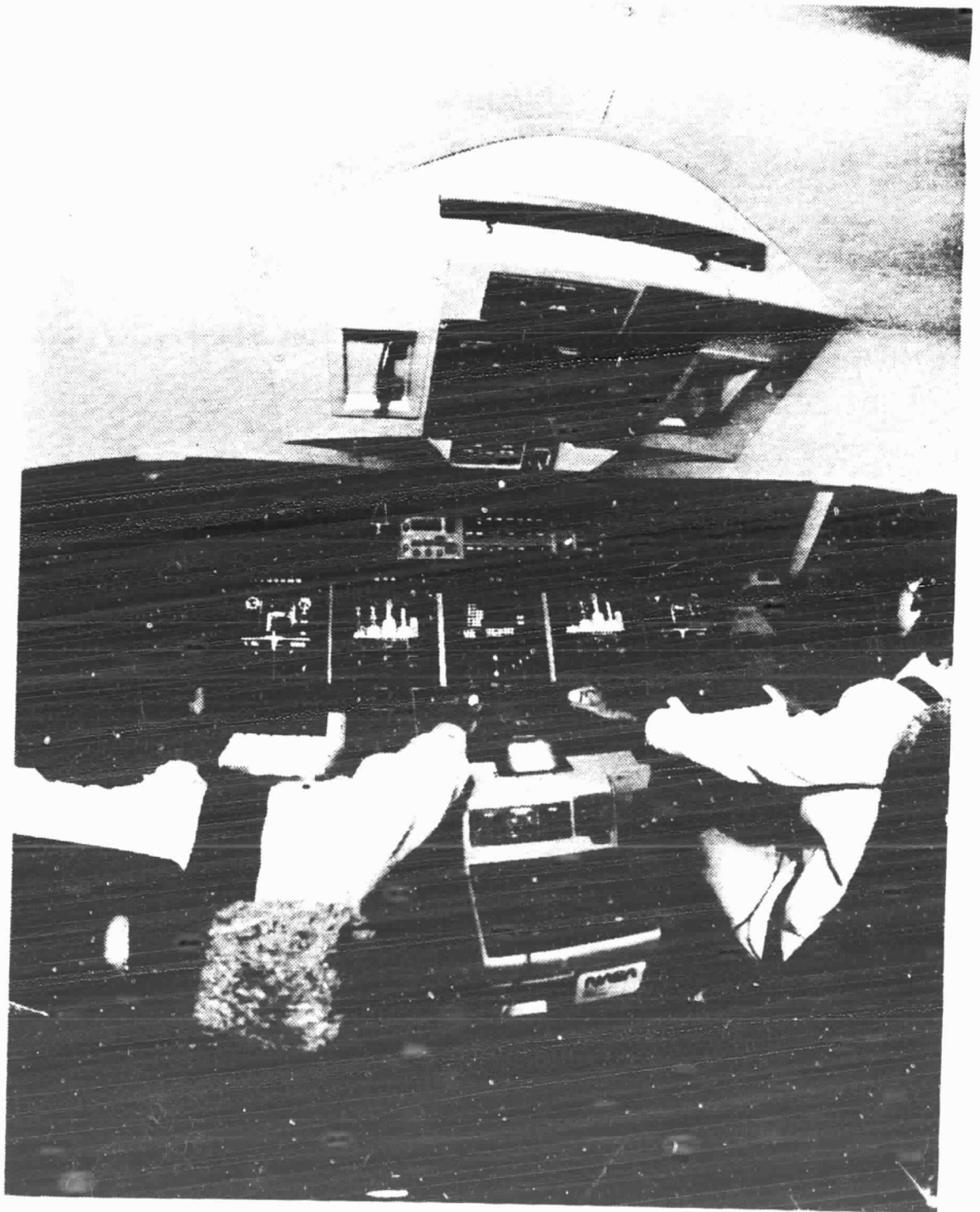
Figure 2. ACFS Flight Station Layout

18

LINK-DEBUG PAGE FILE PHOTO GENERATOR

CYCLE # = 00001C99
FRAME # =   07
CRT #   =   3

```
04 **PERFORMANCE VARIABLES
OFF                      01 EOTFF       TOTAL FUEL FREEZE
40.3947292               02 WTCG        AIRCRAFT CENTER OF GRAVITY
37170.4926               03 ENPRALT     PRESSURE ALTITUDE
185.592136               04 ENIAS       INDICATED AIRSPEED
8066.47656               05 PRTHRUS     THRUST PER ENGINE
109.010786               06 ENQ         DYNAMIC PRESSURE
0.77634946               07 AOCL        LIFT COEFFICIENT
0.05148416               08 AOCD        DRAG COEFFICIENT
3040.78886               09 PRFF        FUEL FLOW PER ENGINE
4.29083346               10 FDALPDG     AIRCRAFT ANGLE OF ATTACK
0.58907346               11 ENMACH      MACH NUMBER
3503.34616               12 TIME        LOCAL- RMFDY    EW 15C5C CPU 4
0.0000000                13 DISTANC     LOCAL- RMFDY    EW 15BF4 CPU 4
12178.2506               14 DRAG        LOCAL- RMFDY    EW 15BF0 CPU 4
12.0532516               15 PSUBS       LOCAL- RMFDY    EW 15C4C CPU 4
-56.500000               16 ENTA        AMBIENT TEMPERATURE
0.37696616               17 TSFC        LOCAL- RMFDY    EW 15C60 CPU 4
1898.09496               18 RANGE       LOCAL- RMFDY    EW 15C58 CPU 4
184992.81                19 WTGRWT      GROSS WEIGHT
0.00000000               20 EODLTMP     TEMP DIFFERENCE FROM STANDARD
/?/
/?/
/?/
```

Figure 3. Performance Variable Debug Page

section of the ACFS flight deck. The variables are updated approximately once per second during ACFS operation. Throughout each profile flown, the simulation was frozen at periodic intervals, and a hard copy of the debug screen was sent to a printer. At the termination of the flight, the data printout was collected and prepared for reduction.

II. STALL CHARACTERISTICS

A. THEORY

Aircraft stall characteristics represent one of the most important parameters to be obtained in a performance evaluation. The aerodynamic lift characteristics of an aircraft are portrayed by the curve of lift coefficient versus angle of attack. For a given aerodynamic configuration, the lift coefficient will increase with angle of attack until the maximum value of lift coefficient is reached. A further increase in angle of attack results in a stalled condition and a subsequent decrease in lift coefficient. Since the maximum lift coefficient corresponds to the minimum speed available in flight, it is an important point of reference. The stall speed of the aircraft in level, one "g" flight is defined by the equation [Ref. 2]:

$$V_S = 17.2 \sqrt{W/(C_{L\ max}\sigma S)} \tag{1}$$

where:

V_S = stall speed (KTAS)

W = gross weight (lbs)

$C_{L\ max}$ = maximum lift coefficient

σ = density ratio

S = wing area (sq. ft.)

21

For an aircraft loaded at one center of gravity (cg) location, the stall will occur at the same coefficient of lift regardless of the aircraft gross weight. Unless large thrust effects are present, the stalling airspeed will vary with the square root of the aircraft gross weight. Another factor which influences stall speed is altitude. As altitude increases, the maximum lift coefficient decreases because of Reynolds number and Mach number effects. These factors account for an increase in stall speed as altitude increases; however, this effect is usually negligible for altitudes below 10,000 feet.

The primary purpose of high lift devices such as wing flaps and slats is to increase the $C_{L\ max}$ and to reduce the stall speed of the aircraft. As a result, normal take-off and approach speeds can be reduced when the high lift devices are deployed. However, the contribution of high lift devices must be considerable to cause a large reduction in stall speed. For example, in order to reduce the stall speed by 30 percent, a 100 percent increase in $C_{L\ max}$ must be achieved through the use of high lift devices. [Ref. 2]

B. TEST PROCEDURES

The objective of stall speed testing is to accurately define the steady state stall speed. However, this stall speed must be approached at a defined airspeed deceleration rate. The FAA requires that the airspeed bleed rate at the stall condition be one knot per second or less [Ref. 3].

22

Airspeed bleed rates in excess of one knot per second can adversely effect the test results due to the presence of non-steady aerodynamic flow effects. This deceleration rate was established as a primary requirement during the stall testing.

All approach configuration stall test profiles were flown at a gross weight of 185,000 pounds and at an altitude of 5000 feet. The flight technique utilized was to trim the aircraft at approximately 200 KIAS for straight and level flight. The power was then reduced accordingly so as to establish an airspeed bleed rate of one knot per second or less. Back stick was applied to maintain altitude, and care was taken not to trim into the stall. The primary attitude reference was provided by cockpit instrumentation since the ACFS night visual simulated horizon was insufficient for adequate attitude information. At approximately every five knots of reduction in airspeed, the simulation was frozen and a hard copy of the debug screen recorded. The first indication of stall onset in the cockpit was a noticeable requirement for increased back stick in order to maintain altitude, followed immediately by a corresponding increase in the rate of descent. There appeared to be very little warning via visual clues of this nose down pitching moment. Recovery from the stall was initiated by simply reducing the back stick pressure to decrease the angle of attack. Four approach configurations were flight tested (all four with

23

landing gear down): landing flaps (40°), take-off/approach
flaps (27°), lift tailoring flaps (5°), and flaps up (0°).

"Clean" stall profiles, with landing gear and flaps up,
were also conducted at altitudes of 5000, 20,000, 30,000,
and 41,000 feet. The methods of entry into the stall and
data collection were the same as mentioned above. During
all stall flight profiles flown, the on-board fuel was
frozen via a debug screen command. This effectively
eliminated any variation in aerodynamic parameters due to
changes in gross weight.

C. TEST RESULTS

Figure 4 shows the approach configuration lift curve for
the ACFS. These plots of lift coefficient versus angle of
attack for the four selectable flap settings clearly
demonstrate the primary purpose of high lift devices--to
increase the maximum coefficient of lift, thus reducing the
stall airspeed. As the flap deflection is increased, both
the $C_{L\ max}$ and its corresponding angle of attack increase.
It can also be noted that the slope of the linear portion of
the lift curve decreases slightly with a reduction in flap
deflection. The lift curve slope of a wing is directly
proportional to that wing's area. As described in detail in
Chapter VI, the fowler flaps on the ACFS effectively
increase the wing area when deployed. As the flap
deflection is decreased, the wing area decreases, thus
decreasing the slope. [Ref. 4]

24
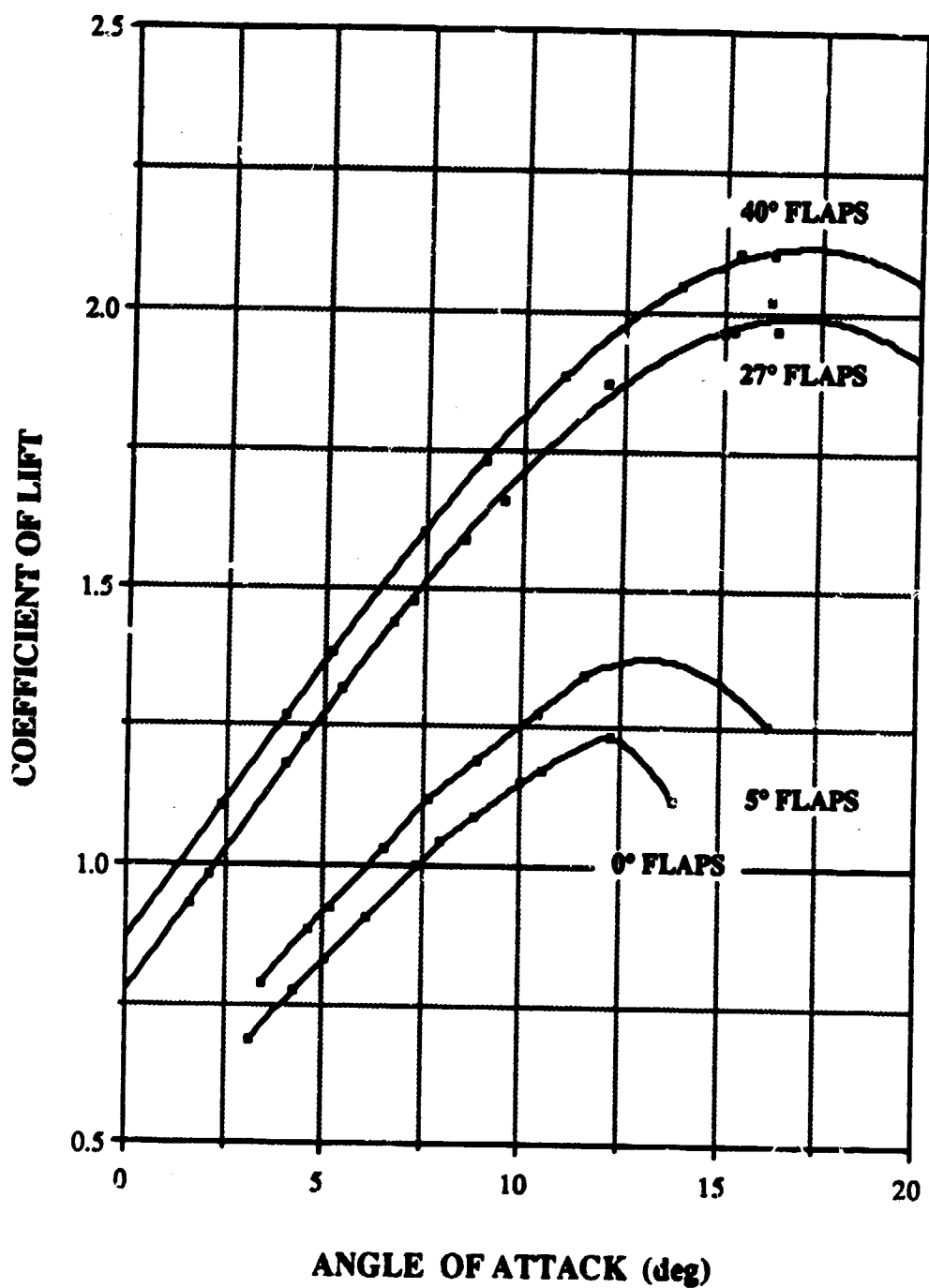
Figure 4.   Approach Configuration Lift Curve

25

The lift characteristics in the clean configuration are shown in Figure 5. As the altitude is increased, the $C_{L\ max}$ and the associated angle of attack both decrease. Since $C_{L\ max}$ is in the denominator of equation (1), it follows that the stall speed will increase with an increase in altitude.

The stall airspeeds for both approach and clean configurations are depicted in Figures 6 and 7, respectively. In the approach configuration, the effect of gross weight on stall speed is evident. At a flap setting of 40°, for example, a 22% increase in weight from 150,000 to 185,000 pounds produces a 10% increase in stall speed. The data tend to verify a useful rule of thumb that expresses the weight effect on stall speed--a 2% change in weight causes a 1% change in stall speed [Ref. 2]. Figure 7 illustrates the effect of altitude on stall speed in the clean configuration. At a gross weight of 220,000 pounds, the indicated stall speed increases from 156 KIAS at 5000 feet to 160 KIAS at 41,000 feet. (Indicated airspeed is used here because that is the type of airspeed readout directly presented to the aircrew in the cockpit.) For comparison, the same two stall speeds in terms of true airspeed are 167 KTAS and 337 KTAS, respectively. The true airspeeds give a more positive indication of the effect of altitude on stall speed.
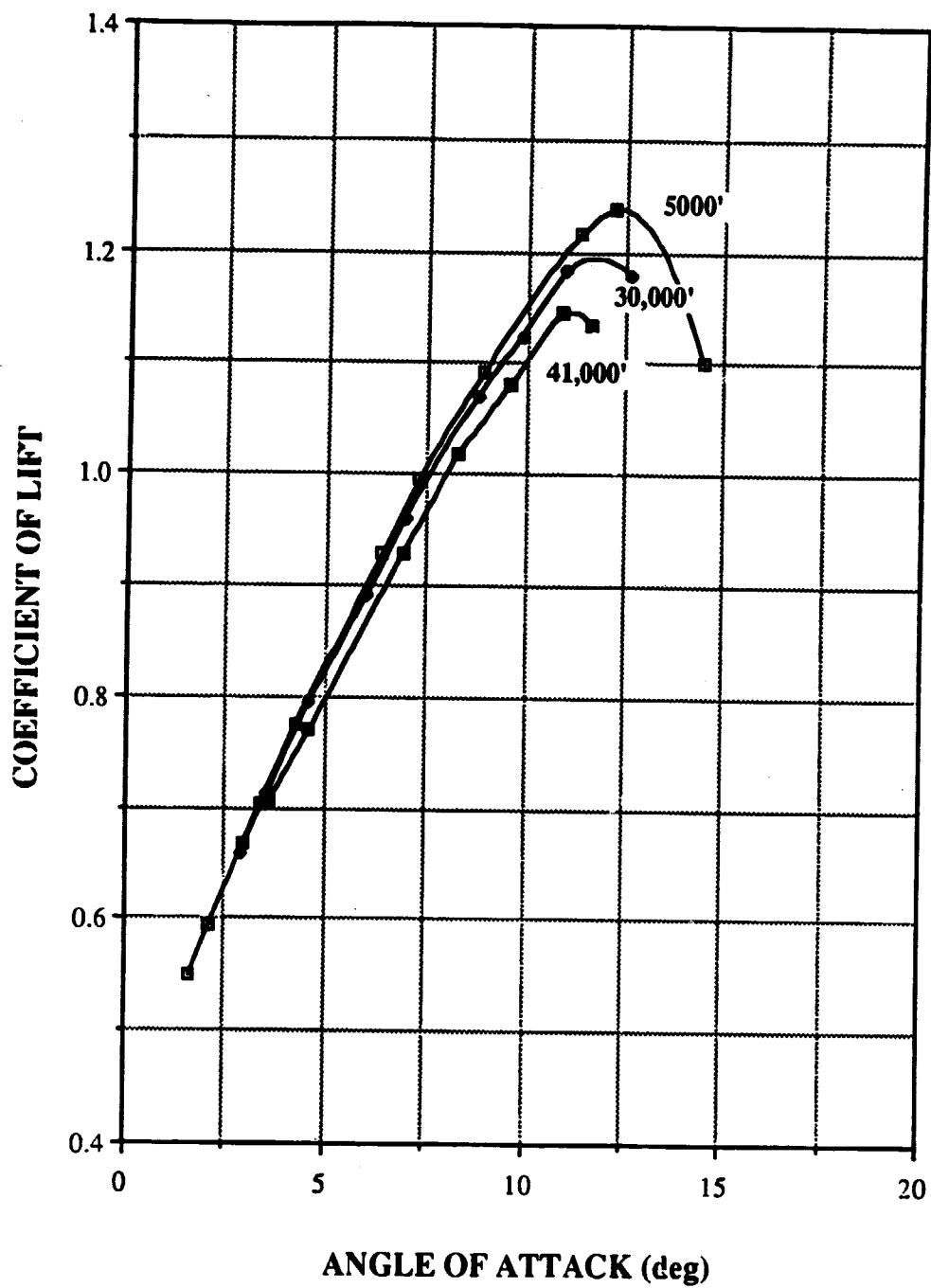
Figure 5.   Clean Configuration Lift Curve

ACFS STALL AIRSPEEDS APPROACH CONFIGURATION				
GROSS WEIGHT (lbs)	FLAP SETTING			
	40°	27°	5°	0°
	KNOTS (IAS)			
150000	99	101	123	128
165000	103	106	129	135
185000	109	112	137	143
200000	114	116	142	149
220000	119	122	149	156

Figure 6.   Approach Configuration Stall Speeds

ACFS STALL AIRSPEEDS CLEAN CONFIGURATION				
GROSS WEIGHT (lbs)	ALTITUDE			
	5000'	10,000'	20,000'	30,000'
	KNOTS (IAS)			
150000	128	129	130	132
165000	135	135	136	138
185000	143	144	145	146
200000	149	147	150	152
220000	156	156	158	160

Figure 7.   Clean Configuration Stall Speeds

III. TAKE-OFF PERFORMANCE

A. THEORY

The take-off phase of flight is a condition of accelerated motion from the beginning of the take-off roll to the point of rotation and lift-off. The key factors to be considered during take-off are:

1. The take-off velocity, which is normally a function of the stall speed.

2. The acceleration during take-off roll, which varies directly with the imbalance of forces and inversely with the mass of the aircraft.

3. The take-off distance, which is a function of both acceleration and velocity. [Ref. 5]

The minimum take-off distance is a parameter of primary interest in the operation of any aircraft. For this flight profile, the aircraft must lift-off at a minimum safe speed which provides a sufficient margin above the stall speed, satisfactory control of the aircraft, and a desired initial rate of climb.

The definitions of velocity and acceleration are:

$$V = \frac{ds}{dt} \tag{2}$$

$$a = \frac{dV}{dt} \tag{3}$$

Combining equations (2) and (3) yields:

$$ds = \frac{V \, dV}{a} \qquad (4)$$

By integrating equation (4) between any two arbitrary speeds and distances, the following equation results:

$$s_y - s_x = \int_{V_x}^{V_y} \frac{V \, dV}{a} \qquad (5)$$

When considering the take-off ground run situation, the expression $s_y - s_x$ can be replaced by S_g (ground distance), V_x goes to zero (no wind), and V_y is replaced by V_{lof} (lift-off speed). The equation now becomes:

$$S_g = \int_{0}^{V_{lof}} \frac{V \, dV}{a} \qquad (6)$$

The acceleration of an aircraft during the ground run may be determined by considering the forces acting on the aircraft, as shown in Figure 8. The aircraft is seen to be under the influence of lift, drag, thrust, weight, and ground friction forces. Within the scope of this evaluation, the runway inclination (ϕ) was set at zero and the coefficient of friction (μ) was set at .02, the value for dry concrete.

A balance of forces yields:

$$F_a = Ma = \left(\frac{W}{g}\right) a \qquad (7)$$

30
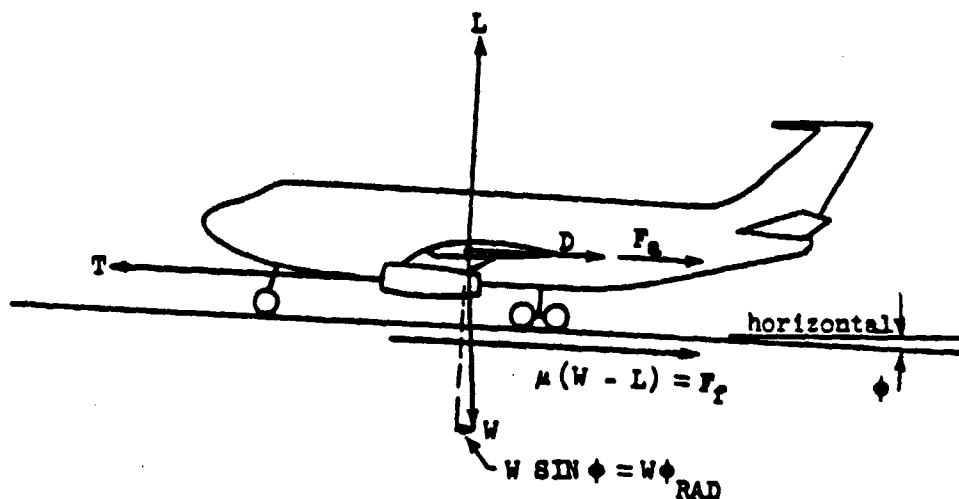
Figure 8. Forces Present During Take-Off Roll

Thus,

$$T - D - \mu(W-L) = \left(\frac{W}{g}\right)a \tag{8}$$

Rearranging equation (8) produces:

$$a = \left(\frac{g}{W}\right)[(T-\mu W) - (C_D-\mu C_L)qS] \tag{9}$$

Now substituting equation (9) into equation (6) results in:

$$S_g = \int_0^{V_{lof}} \left(\frac{W}{g}\right)\frac{V\ dV}{[(T-\mu W) - (C_D-\mu C_L)qS]} \tag{10}$$

This is the general expression for take-off distance. To integrate equation (10), the variation of thrust, weight, drag, and lift with velocity must be determined. In general, thrust is a function of velocity, air temperature,

31

and pressure; weight will be very nearly constant for the ground run; and C_D and C_L will not vary throughout the ground run since the aircraft attitude remains constant until rotation. [Ref. 6]

B. TEST PROCEDURES

The ACFS take-off profiles were conducted at sea level at gross weights of 150,000, 185,000, and 220,000 pounds. The outside air temperature was set at -5°C, 15°C, and 35°C. This ensured that the effects of gross weight and density altitude on take-off performance could be completely observed.

Once the simulator was configured for the proper gross weight and temperature, the parking brake was set, the nose trim was set at zero, and the power levers advanced to an engine pressure ratio (EPR) setting of 1.5. This setting was chosen to allow for a standardized power setting that could be applied during each of the nine runs. Prior to brake release, the simulation was frozen, and a hard copy of the debug page was recorded. The brakes were then released simultaneously as the simulator was taken out of the freeze mode. This procedure ensured that the simulator frame time constant commenced running just as the aircraft started to roll. The simulation was again frozen at incremental airspeeds of 20 to 25 knots between brake release and lift-off. No elevator commands were applied, and the aircraft accelerated until rotation and lift-off. This

ensured that the actual lift-off speed would be well in excess of the calculated take-off speed, thus providing data points up to and beyond the take-off speed.

C.   TEST RESULTS

In Chapter II, stall airspeeds were computed for the various approach configurations. These stall speeds were then used to establish speeds at which the aircraft will rotate and take-off, using the following criteria for transport aircraft [Ref. 7]:

$$V_2 = 1.2 \ V_s \qquad\qquad (11)$$

and

$$V_r = 1.145 \ V_s \qquad\qquad (12)$$

where

V_s = stall airspeed

V_2 = take-off climb airspeed

V_r = rotation airspeed

The next step in the data reduction process was to plot take-off velocity as a function of time from the data points on the debug page printouts (Figures 9, 10, and 11). It can easily be seen from the plots that the take-off roll acceleration decreases with an increase in outside air
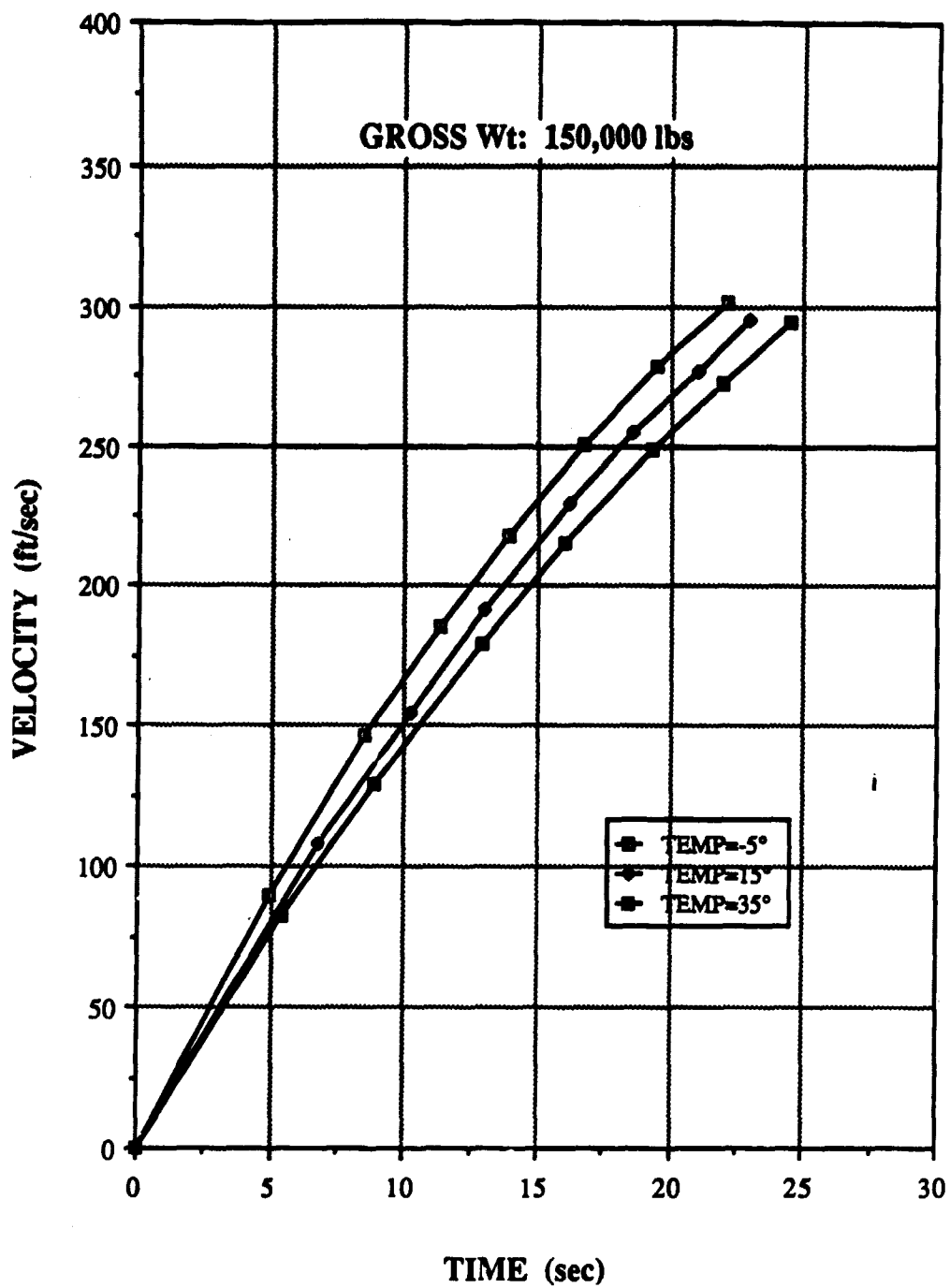
Figure 9.   Take-Off Roll Acceleration (150,000 lbs)

34
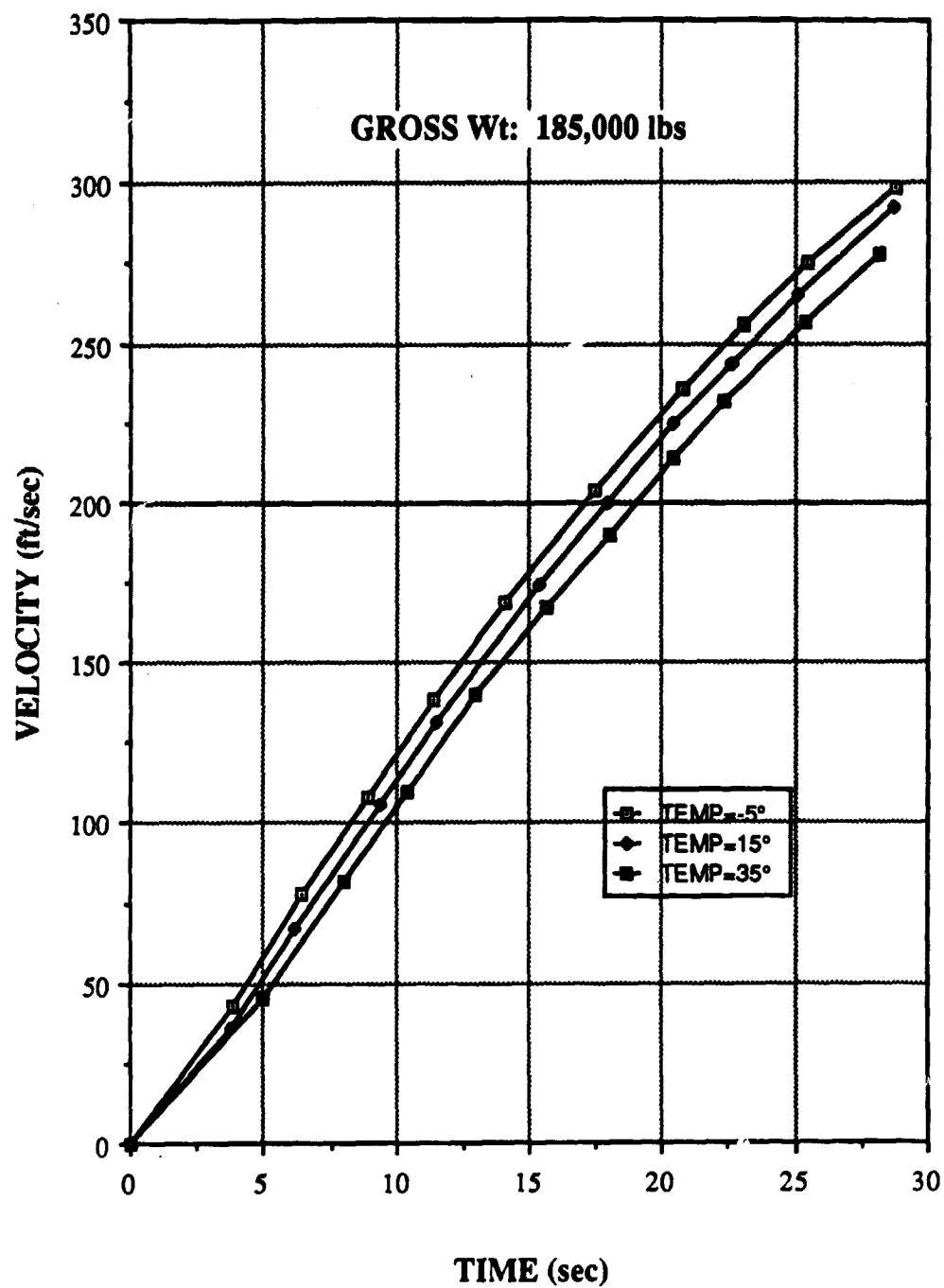
Figure 10. Take-Off Roll Acceleration (185,000 lbs)
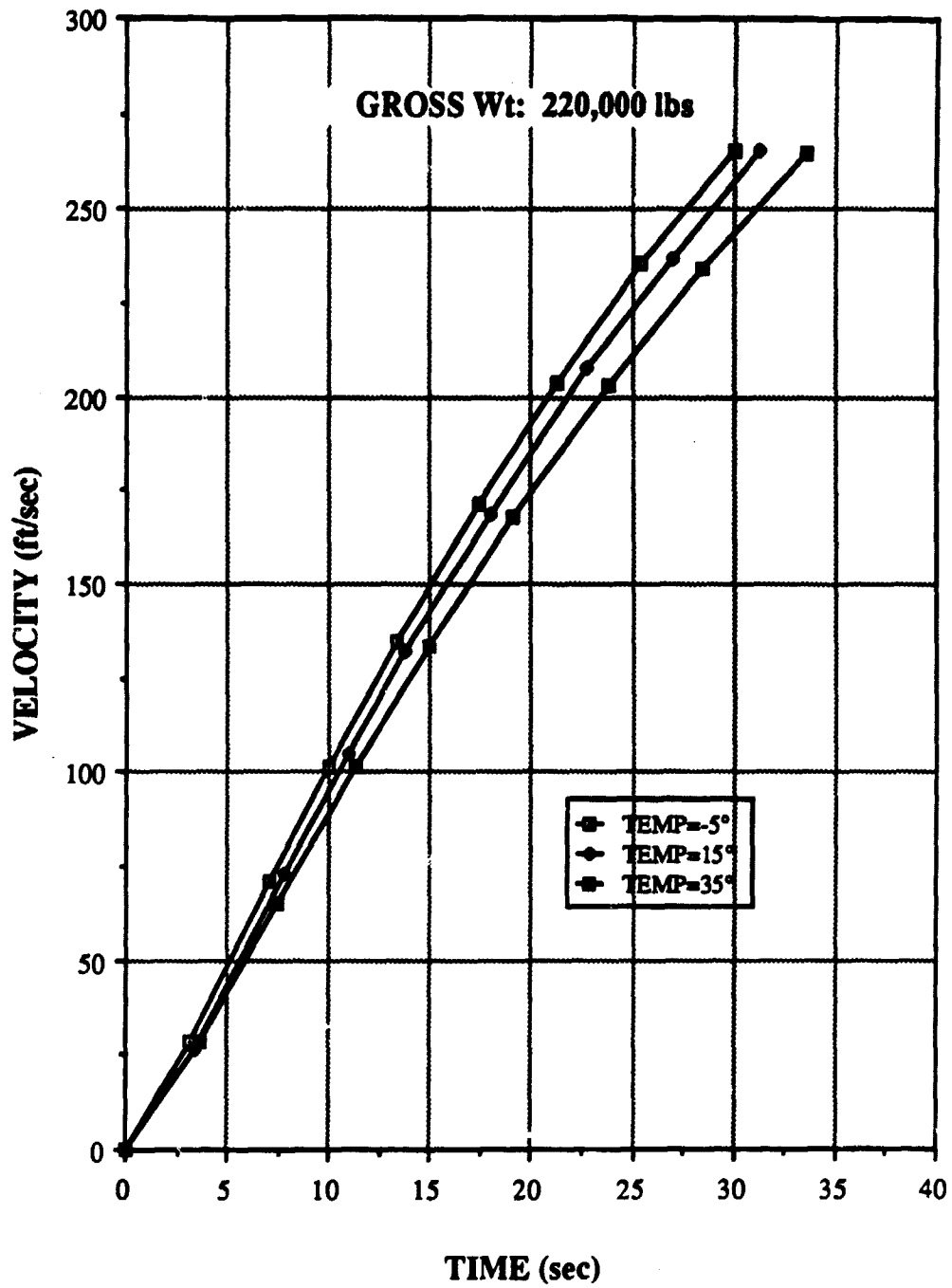
Figure 11.   Take-Off Roll Acceleration (220,000 lbs)

temperature (for a given gross weight at a given pressure altitude). Next, the take-off distance for each case was determined. Using the example of a 150,000 pound aircraft at -5°C, the following equation was produced with the aid of a graphics package software third-order polynomial curve-fitting routine to approximate the curve in question:

$$V = -.03 + 19.966t - .341t^2 + .0025t^3 \qquad (13)$$

Now, since

$$s = \int V \, dt \qquad (14)$$

where

$$s = \text{distance}$$

an equation showing distance as a function of time can be determined by integrating equation (13) to obtain:

$$s = -.03t + 9.983t^2 - .1137t^3 + .00068t^4 \qquad (15)$$

For a gross weight of 150,000 pounds at -5°C, V_2 was calculated to be 121 KIAS. This converts to 204.4 ft/sec. Substituting this value into equation (13) and solving for time by iteration yields a value of 12.7 seconds. This is

37

the time it takes to accelerate from the brake release condition to an airspeed of 121 KIAS. This time of 12.7 seconds can now be substituted into equation (15) to produce the take-off roll distance, which in this case is 1493 feet. By means of this process, take-off roll distances were calculated for the three gross weights of 150,000, 185,000, and 220,000 pounds, at outside air temperatures of -5°C, 15°C, and 35°C.

In order to provide performance data that covered the entire operating envelope of the ACFS, it was determined that performance parameters would be required for the additional selectable gross weights of 165,000 and 200,000 pounds. Additionally, all five gross weight selections should be examined at pressure altitudes up to 5000 feet. To calculate these numbers by means of additional test profiles in the ACFS would have entailed many additional hours in the simulator. Instead, approximation methods were investigated to determine if acceptable results could be arrived at computationally, rather than experimentally. The fact that the take-off roll acceleration is not constant, as indicated by the non-linear curves in Figures 9, 10, and 11, quickly eliminated several common approximation methods.

Lan and Roskam [Ref. 6] describe an approximation method that is limited only by the assumption that the thrust varies linearly with the velocity squared. Figure 12 was constructed using data from the case of the 150,000 pound
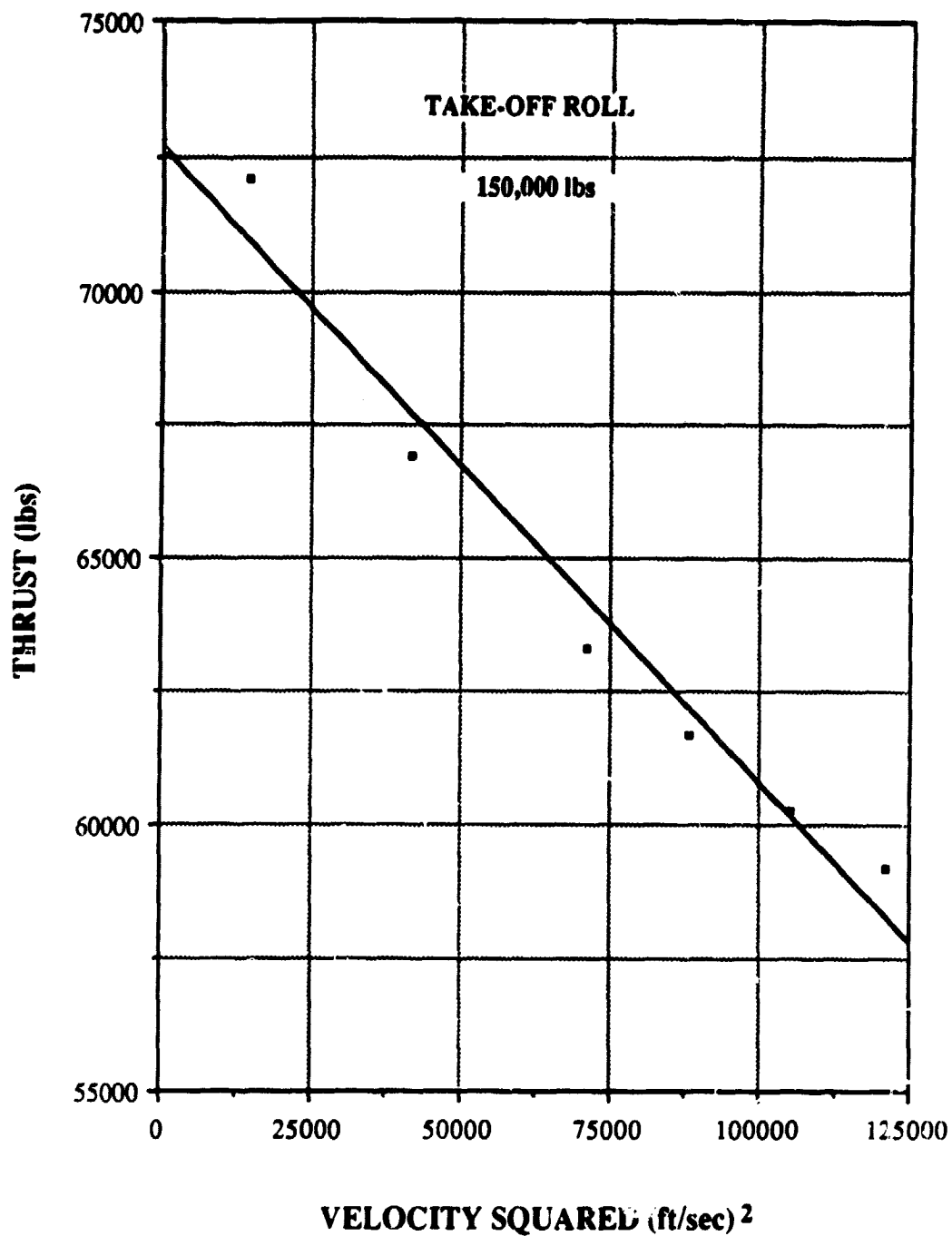
Figure 12. Thrust During Take-Off Roll

aircraft at -5°C. It indicates that there is in fact a nearly linear relationship between thrust and velocity squared during take-off. The approximation method is based on the following equation:

$$S_g = \frac{W}{2g} \frac{V_{lof}^2}{F_m} \qquad (16)$$

wher. F_m can be regarded as the average net force for acceleration:

$$F_m = F_s \frac{1 - \dfrac{F_{lof}}{F_s}}{\ln \dfrac{F_s}{F_{lof}}} \qquad (17)$$

with:

$$F_s = T - \mu W \quad \text{at} \quad V = 0 \qquad (18)$$

$$F_{lof} = T - D - \mu(W-L) \quad \text{at} \quad V = V_{lof} \qquad (19)$$

To verify the accuracy of this method, the computed results from equation (16) were compared with those determined experimentally in the simulator. Take-off distances (S_g) were computed for each of the nine previous take-off profiles, and all computed distances were found to be within 4% of the actual profile distances. Therefore, it

was determined that this method would indeed provide adequate result* for inclusion in this report. Figure 13 was constructed from existing data so that stall speeds for 165,000 and 220,000 pounds could be extrapolated. The data verified that both C_L and C_D remained constant throughout the take-off roll. The thrust available at brake release was also constant for a given temperature. Through the use of equation (16), it war ... ... ble to compute S_g for gross weights of 165,000 ... ... pounds, based on the acquisition of the above ... ... .ables and constants.

A similar procedure was ... ... ed in order to produce performance parameters for varying pressure altitudes. A change in pressure altitude directly affects two variables: thrust and dynamic pressure (q) [Ref. 2]. With an increase in altitude, a turbojet's thrust output, for a constant engine RPM, decreases (Figure 14). This thrust ratio (as shown on the y-axis) can be used to directly determine the corresponding thrust at a particular pressure altitude. The dynamic pressure varies directly with the density ratio as pressure altitude increases. This relationship was used to produce the dynamic pressure corresponding to a particular pressure altitude. These variables, along with the previously mentioned constants, were applied to equation (16) in order to produce performance data for various pressure altitudes. To verify the accuracy of this method with regard to varying pressure altitudes, two profiles each

41
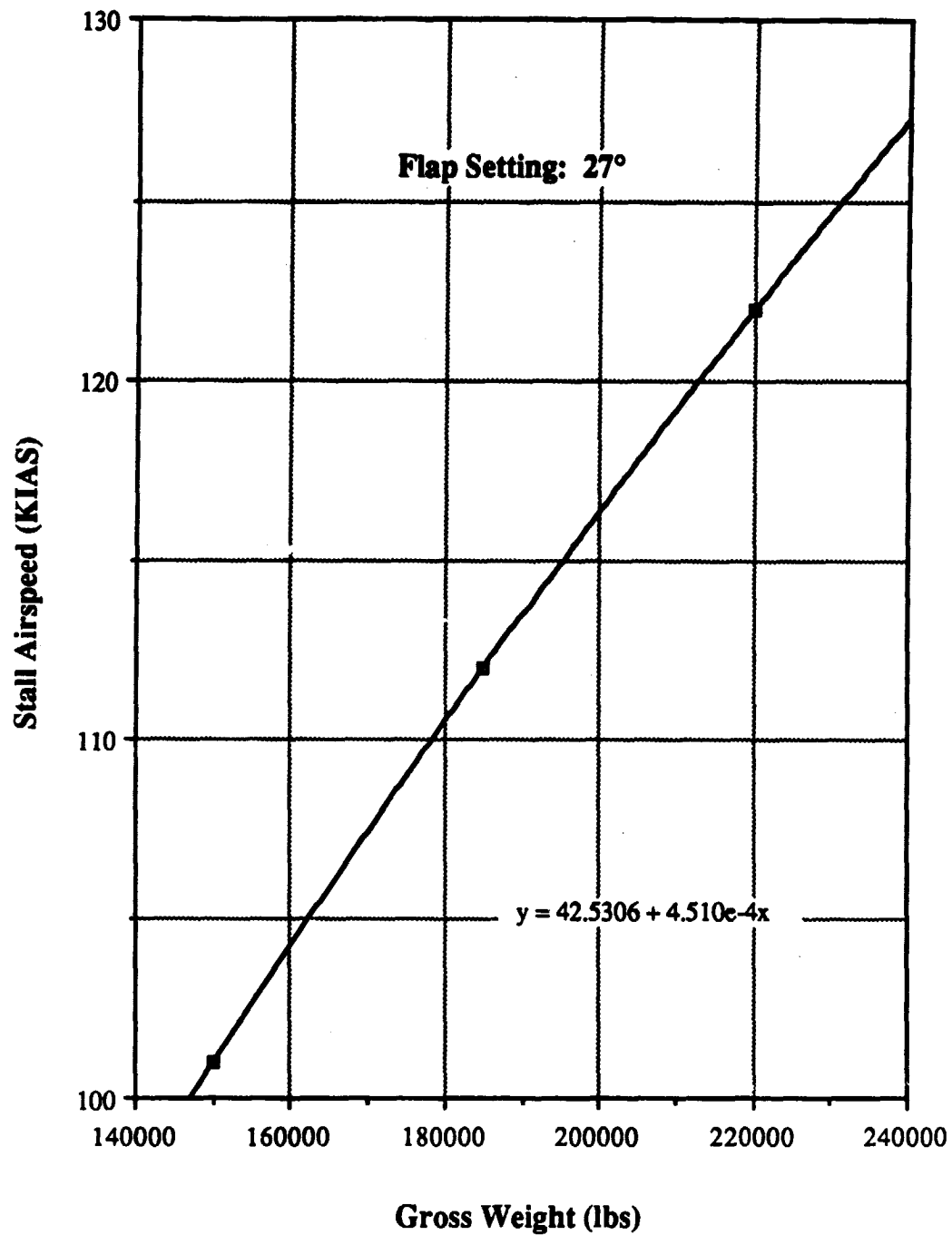
Figure 13. Stall Airspeed vs. Gross Weight
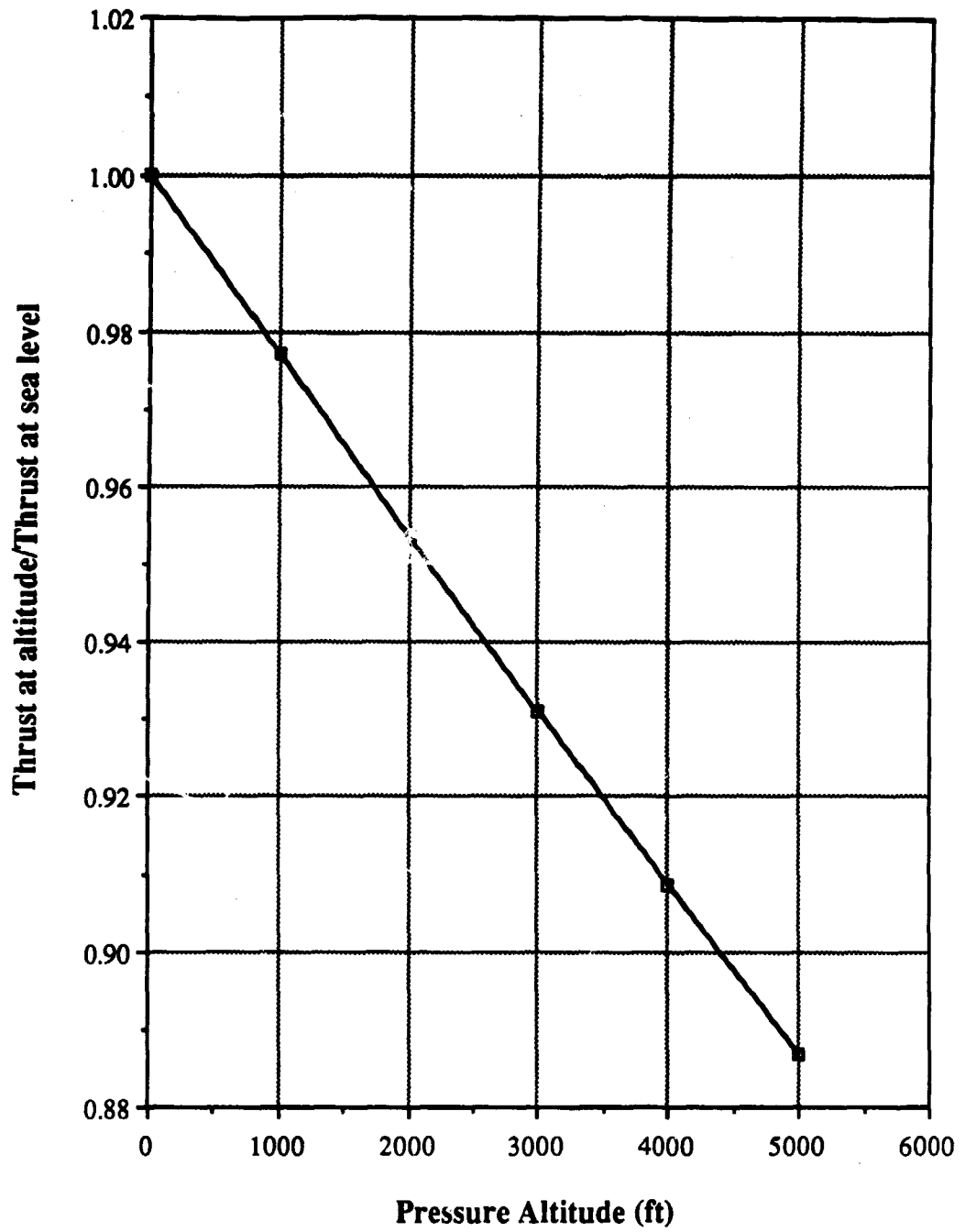
Figure 14.   Thrust Ratio vs. Altitude

43

at altitudes of 3000 and 5000 feet were conducted in the simulator and the experimental results compared to those computed with equation (16). In each case, the computed results were within 5% of the experimental values.

Figure 15 contains take-off performance data for a pressure altitude of sea level. Similar figures for altitudes of 1000 through 5000 feet are contained in Appendix C.

ACES TAKE-OFF PERFORMANCE DATA

TRIM : zero

PRESSURE ALTITUDE: sea level

GEAR: down
FLAPS: T/O

TAKE-OFF GROSS WT (lbs)	OUTSIDE AIR TEMPERATURE (°C)								
	-15° to 4°			5° to 25°			26° to 46°		
	Vr	V2	T/O DIST	Vr	V2	T/O DIST	Vr	V2	T/O DIST
150,000	116	121	1403	116	121	1512	117	122	1611
165,000	121	127	1775	121	127	1838	122	128	1918
185,000	128	135	2355	128	135	2391	129	136	2490
200,000	133	139	2848	133	139	2873	134	140	3072
220,000	140	147	3590	140	147	3695	141	148	4005

Figure 15.   Take-Off Performance Data

45

IV. CLIMB PERFORMANCE

A. THEORY

In analyzing climb performance, it is useful to consider the aircraft from the standpoint of total energy (TE), which is the sum of potential (PE) and kinetic (KE) energies. The total energy of an aircraft at a given weight (W), airspeed (V), and altitude (h) is [Ref. 8]:

$$TE = KE + PE = Wh + (\frac{W}{2g})V^2 \tag{20}$$

Dividing through by W defines the energy height:

$$Eh = \frac{TE}{W} = h + \frac{V^2}{2g} \tag{21}$$

Energy height, or specific energy, can also be interpreted as energy altitude; that is, the altitude which could be obtained if all the kinetic energy were perfectly converted to potential energy. Differentiating equation (21) produces:

$$\frac{dE_h}{dt} = \frac{dh}{dt} + (\frac{V}{g})\frac{dV}{dt} \tag{22}$$

Consider the aircraft in Figure 16 in climbing flight where the thrust (T) is assumed to be along the flight path:
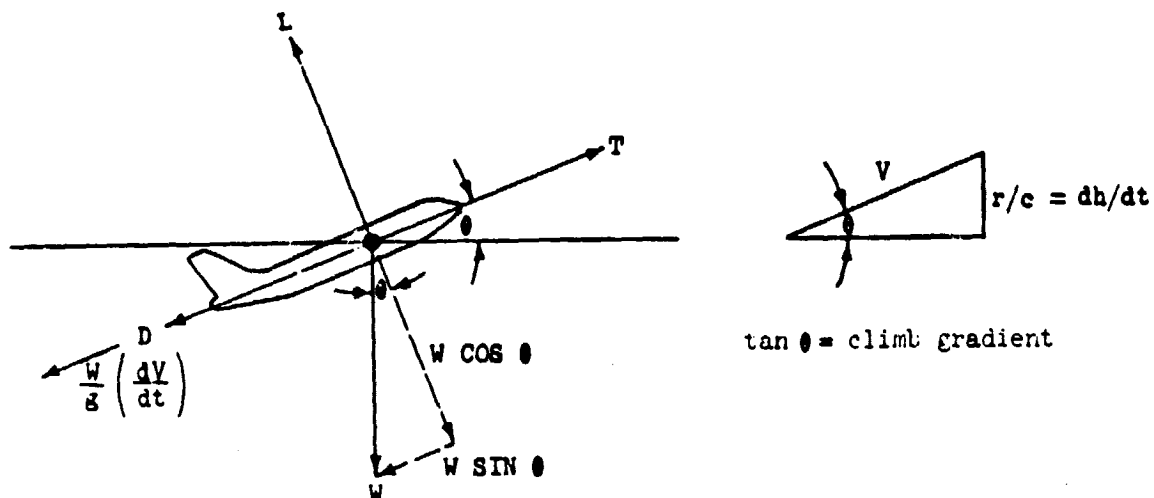
Figure 16.   Free Body Diagram

Summing the forces along the flight path direction produces:

$$F - D - W \cos \theta = \left(\frac{W}{g}\right) \frac{dV}{dt} \tag{23}$$

Rearranging:

$$\sin \theta + \left(\frac{1}{g}\right) \frac{dV}{dt} = (T-d)W \tag{24}$$

Noting that:

$$\sin \theta = \frac{\frac{dh}{dt}}{V} \tag{25}$$

47

Substituting equation (25) into (24) and multiplying by V yields:

$$\frac{dh}{dt} + \left(\frac{V}{g}\right)\frac{dV}{dt} = \frac{V(T-D)}{W} \qquad (26)$$

There now exists an expression for the aircraft's excess power:

$$V(T - D)$$

With regard to equation (22), specific excess power can be defined as:

$$P_s = \frac{V(T-D)}{W} = \frac{dh}{dt} + \left(\frac{V}{g}\right)\frac{dV}{dt} \qquad (27)$$

The flight profile utilized to determine the climb performance of the ACFS was the level acceleration run. The level acceleration profiles provided necessary data to determine the variation of excess power with airspeed.

B. TEST PROCEDURES

Level acceleration flight profiles were conducted at a gross weight of 185,000 pounds at the following altitudes: 5000, 10,000, 20,000, 30,000, 35,000, 37,000, 39,000, and 41,000 feet. For comparison purposes, additional runs were made at gross weights of 150,000 and 220,000 pounds at altitudes between 35,000 and 41,000 feet.

During all acceleration runs, a total fuel freeze was enabled to eliminate the problem of accounting for variations in gross weight during testing. At each selected altitude, the aircraft was established in straight and level flight as close to the minimum flying airspeed as possible. The altitude hold on the autopilot was then engaged, a hard copy of the debug page recorded, and the throttles advanced to full power. After the thrust stabilized, the simulation was frozen and data was recorded at approximately 15 to 25 knot intervals. After each subsequent run, the autopilot was disengaged and the aircraft flown to the next test altitude.

C. TEST RESULTS

The specific excess power derived from each acceleration run conducted was first converted into rate of climb potential by multiplying by a factor of 60, since aircraft rate of climb is normally measured in feet per minute. Figures 17 and 18 depict the rate of climb potential for a 135,000 pound aircraft at altitudes from 5000 to 39,000 feet. The maximum rate of climb decreases accordingly with an increase in altitude, and the Mach number associated with that maximum rate of climb increases with altitude. For example, the maximum rate of climb at 5000 feet is 6600 ft/min at $M = .50$, compared to 560 ft/min at $M = .68$ for an altitude of 39,000 feet.
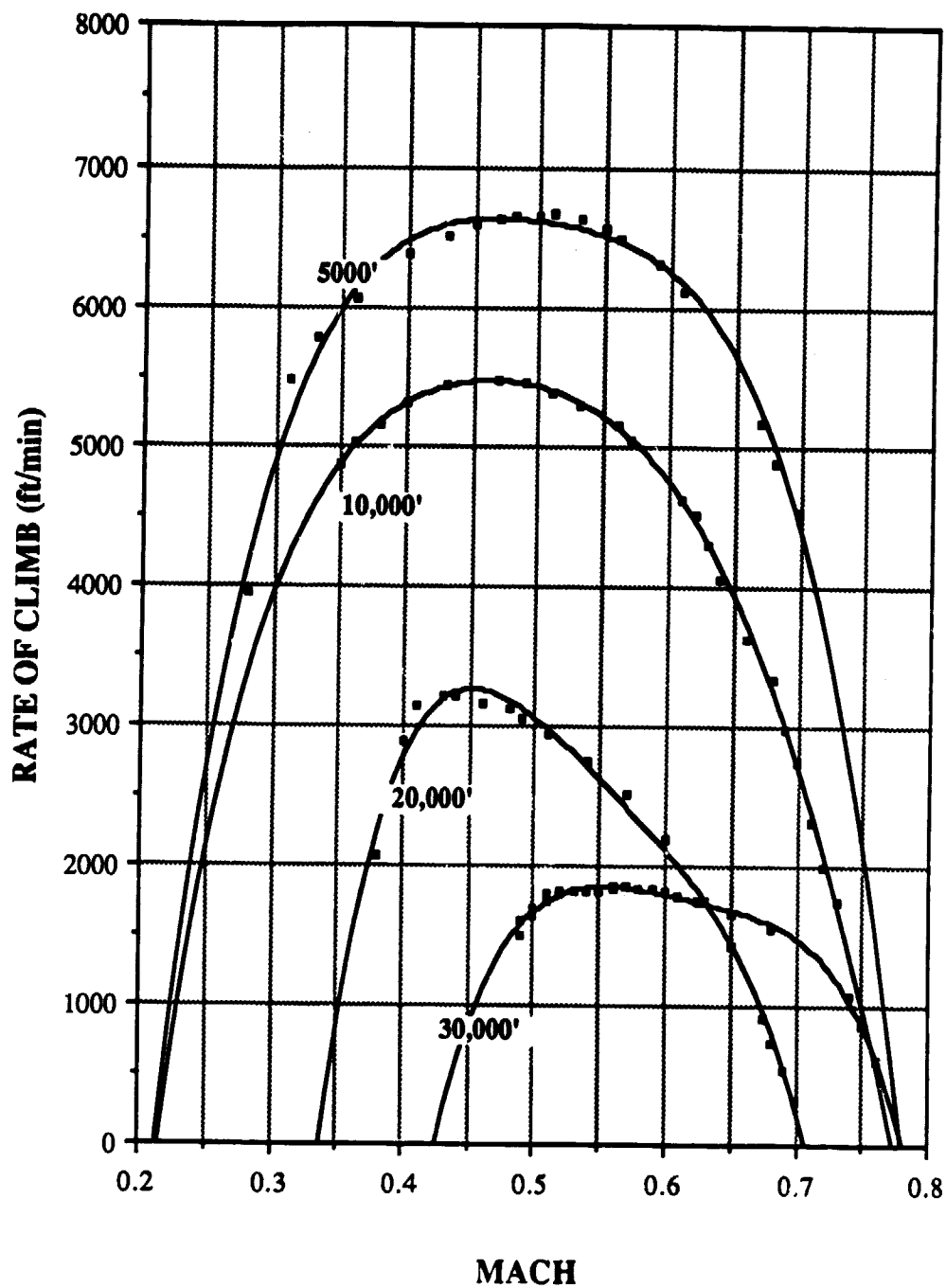
Figure 17. Rate of Climb Potential (185,000 lbs)
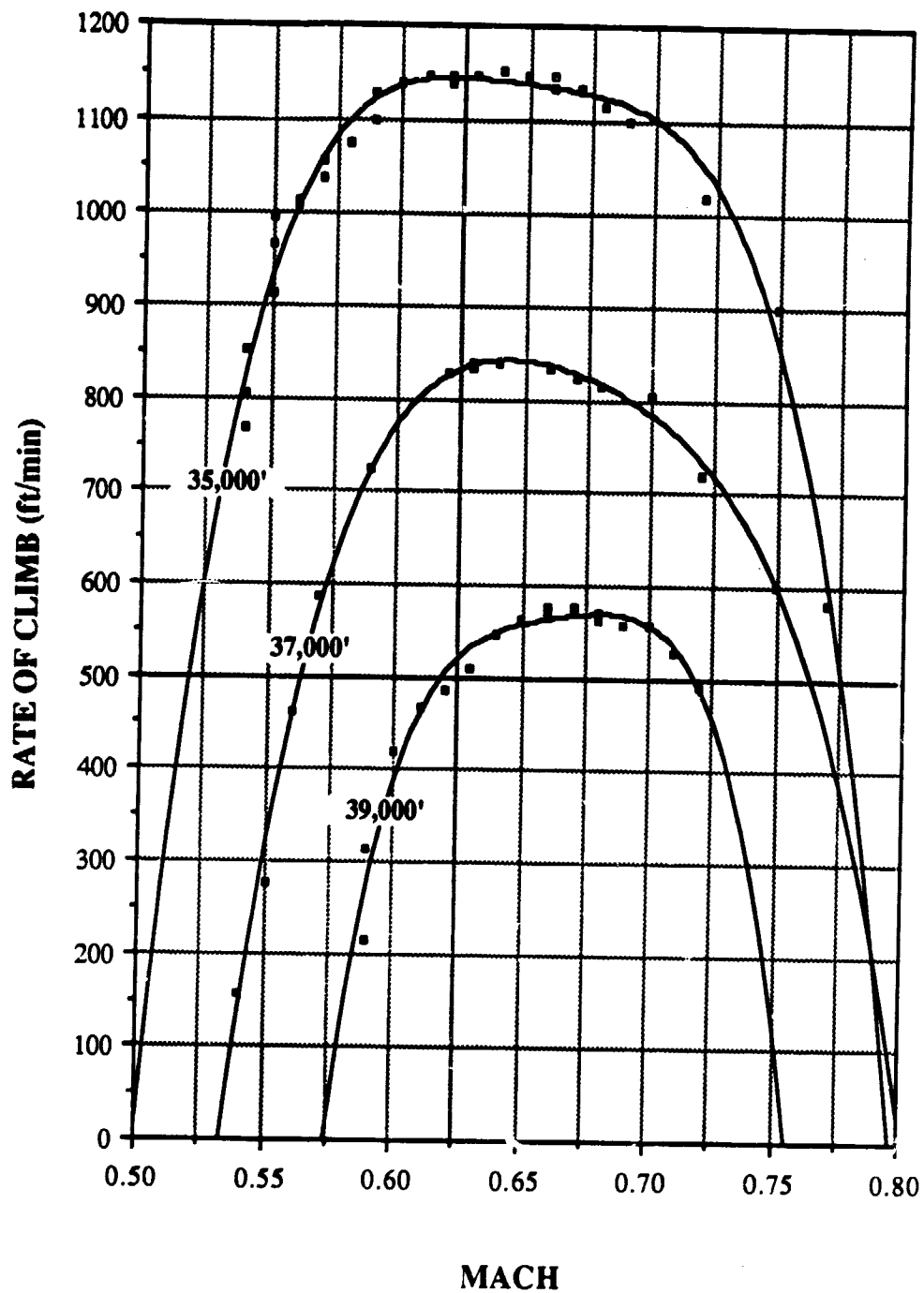
Figure 18. Rate of Climb Potential (185,000 lbs)

Figure 19 demonstrates the effect of gross weight on rate of climb at a given altitude. At 41,000 feet, the maximum rate of climb varies from 1320 ft/min for a 150,000 pound aircraft to 475 ft/min for a 220,000 pound aircraft. Of particular note is the fact that the Mach number associated with the maximum rate of climb for each gross weight (M = .70) is approximately constant.
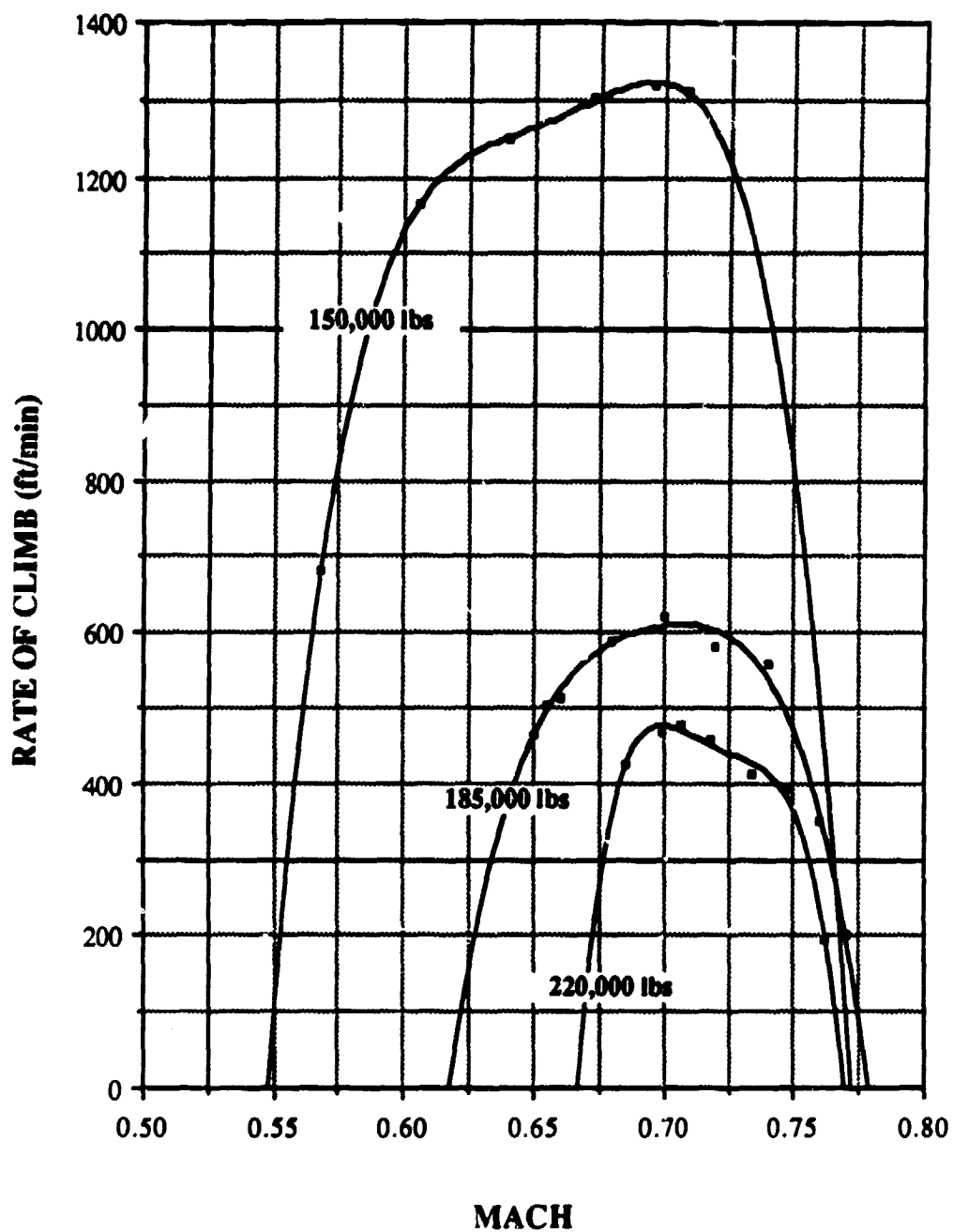
Figure 19. Rate of Climb Potential at 41,000 ft.

V. CRUISE PERFORMANCE

A. THEORY

For an aircraft to fly a given distance, fuel energy must be converted into propulsive work. Since turbojet engines are rated in terms of thrust, the rate of change of aircraft weight can be written as:

$$dW = -TSFC(T\ dt) \tag{28}$$

where:

TSFC = thrust specific fuel consumption in pounds of fuel per second per pound of thrust

T = total thrust.

Hence:

$$\frac{ds}{dW} = \frac{-V}{(TSFC)\ T} \tag{29}$$

and

$$\frac{dt}{dW} = \frac{-1}{(TSFC)\ T} \tag{30}$$

In level, unaccelerated flight, the thrust can be replaced by the drag, and the flight speed can be expressed in terms of W and c_L:

54

$$T = D = W\left(\frac{C_D}{C_L}\right) \tag{31}$$

and:

$$V = \sqrt{(2W)/(\rho S C_L)} \tag{32}$$

Equation (29) can now be written as:

$$\frac{ds}{dW} = \frac{-1}{TSFC} \sqrt{\cdot/(W\rho S)} \left(\frac{\sqrt{C_L}}{C_D}\right) \tag{33}$$

This expression indicates that at a given altitude and weight, the maximum range occurs when $\sqrt{C_L}/C_D$ is a maximum. Integrating equation (6) results in:

$$\begin{array}{ll} \text{Range} \\ \text{(naut. mi.)} \end{array} = \frac{1.675}{TSFC\sqrt{\rho S}} \frac{\sqrt{C_L}}{C_D} \frac{dW}{\sqrt{W}} \tag{34}$$

Equation (34) is known as Breguet's range equation. Note that ρ appears in the denominator. This is a fundamental reason why high cruising altitudes are carefully selected for jet aircraft when good range performance is required. An increase in altitude will also improve engine performance in two respects. First, an increase in altitude (when below the tropopause) will provide lower inlet air temperatures, which in turn reduce the TSFC. A second benefit is due to the increased engine RPM required to furnish cruise thrust. An increase in engine speed to the

normal rated value will reduce the TSFC. The combined effect of these factors defines altitude as the most important item affecting the range of a turbojet aircraft. [Ref. 7]

It should also be noted that when flying at a constant altitude and lift coefficient, equation (32) indicates that the flight speed must be steadily reduced as fuel is consumed in order to maintain a profile for maximum range. While a constant altitude cruise may be necessary due to Air Traffic Control (ATC) restrictions, this flight profile constitutes a certain inefficiency of operation for transport aircraft. If the aircraft were not restricted to a particular altitude, a more efficient flight profile could be flown by maintaining the same C_L and engine RPM and allowing the aircraft to climb as the gross weight decreases.

B. TEST PROCEDURES

In order to provide reliable data, cruise performance test profiles must be evaluated at a constant referred gross weight (W/δ), where δ is the pressure ratio. δ is kept constant by maintaining a constant altitude; in actual flight, however, it is not possible to keep W constant since fuel is continually consumed. Therefore, the ratio is maintained by varying the altitude throughout the profile. In the ACFS, this problem was easily overcome through the

use of the total fuel freeze function, thus maintaining a constant gross weight throughout each profile.

The stabilized flight profile method was used to determine aircraft range. At a gross weight of 185,000 pounds, profiles were conducted at altitudes of 5000, 10,000, 20,000, 30,000, 35,000, 37,000, 39,000, and 41,000 feet. For comparison purposes, profiles were also flown at gross weights of 150,000 and 220,000 pounds at altitudes between 30,000 and 41,000 feet. The stabilized method involved trimming the aircraft in level, unaccelerated flight at several airspeeds between V_{min} and V_{max}. The ACFS was considered to be in unaccelerated flight when the absolute value of the specific excess power (which was displayed on the debug page) was less than one. Each successive trim point, at a given altitude, was obtained by advancing the throttles a small amount and allowing the specific excess power to stabilize within limits. A copy of the debug page was recorded at each trim point. After the final test point at each altitude, the aircraft was flown to the next altitude, and the process repeated.

C. TEST RESULTS

Figures 20 and 21 represent the range performance of the ACFS at a gross weight of 185,000 pounds. These plots indicate that, for a given gross weight, the range increases correspondingly with an increase in altitude, from 1300
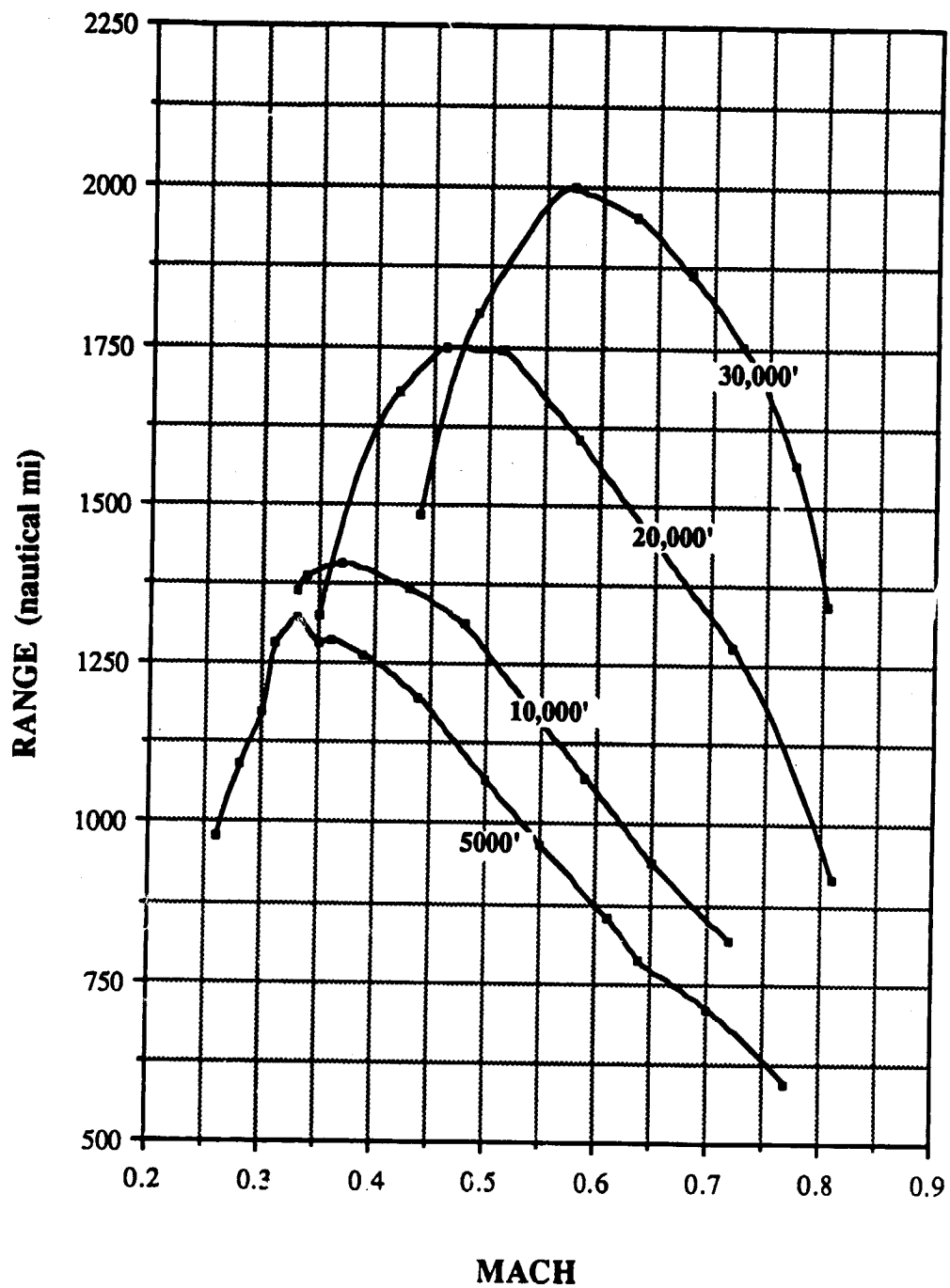
Figure 20. Best Range at Altitude (185,000 lbs)
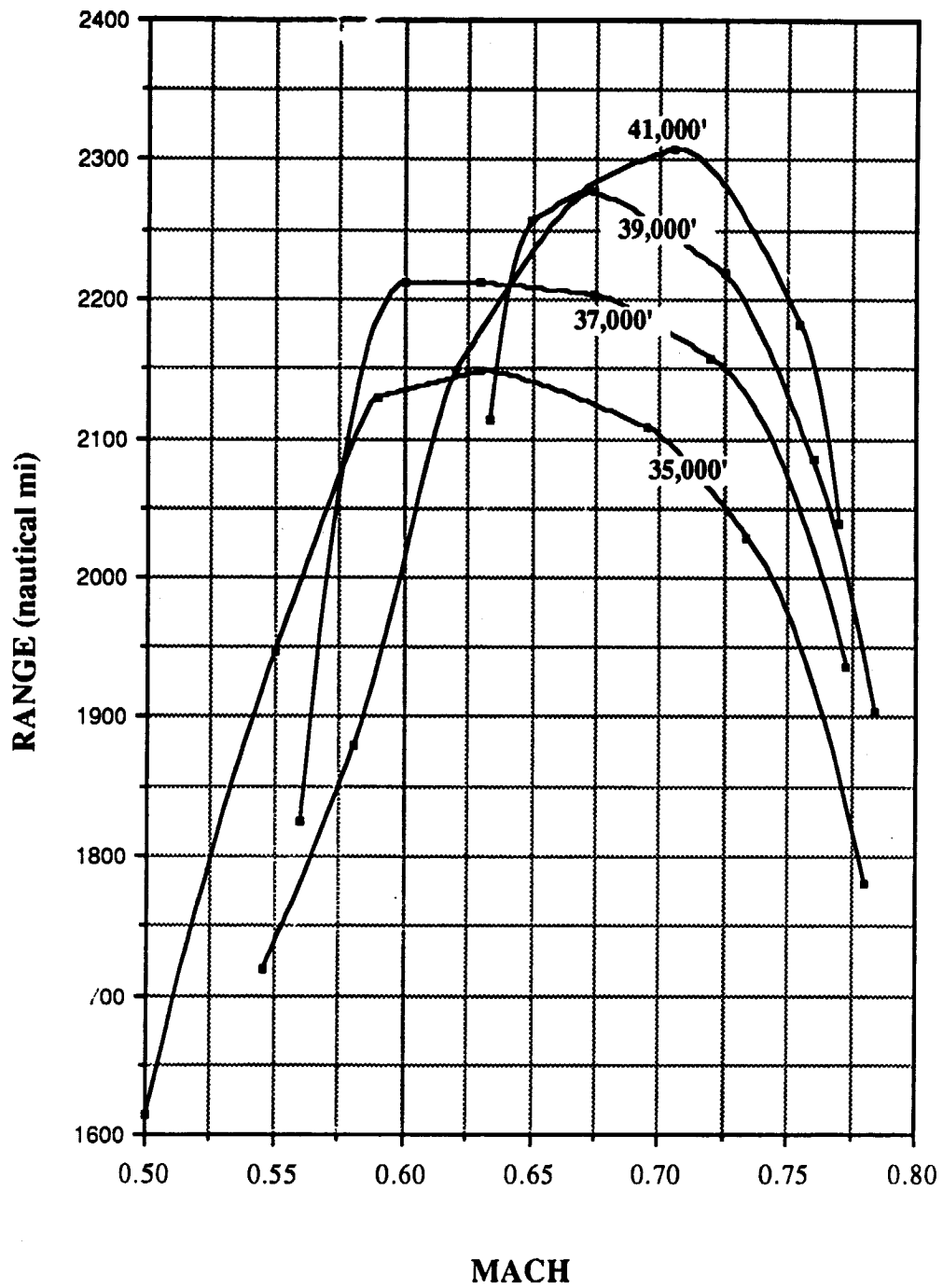
Figure 21. Best Range at Altitude (185,000 lbs)

nautical miles at 5000 feet, to 2300 nautical miles at 41,000 feet. It can also be noted that the best cruise Mach number (flown to achieve maximum range) also increases with altitude, from M = .32 at 5000 feet, to M = .70 at 41,000 feet.

The range performance of the ACFS for gross weights of 150,000 and 220,000 pounds is contained in Figures 22 and 23, respectively. These graphs indicate that for a particular altitude, range increases accordingly with an increase in gross weight (due to the onboard fuel increase). For the 220,000 pound aircraft, it should be noted that the maximum range at 39,000 feet decreased from the value at 37,000 feet. At heavy gross weights, there exists an optimum altitude above which the range will decrease. For the lesser weights, the optimum altitude was at or above the highest altitude tested of 41,000 feet. It should be reemphasized that each gross weight tested contained a preset fuel load, from 10,000 pounds for a gross weight of 150,000 pounds, to 42,500 pounds for a weight of 220,000 pounds (Appendix A).

Figure 24 includes the recommended best cruise Mach number and altitude to achieve maximum range for each selectable gross weight. The values for gross weights of 165,000 and 200,000 pounds were established through interpolation between the tested gross weights. The maximum range did increase linearly for aircraft gross weights of
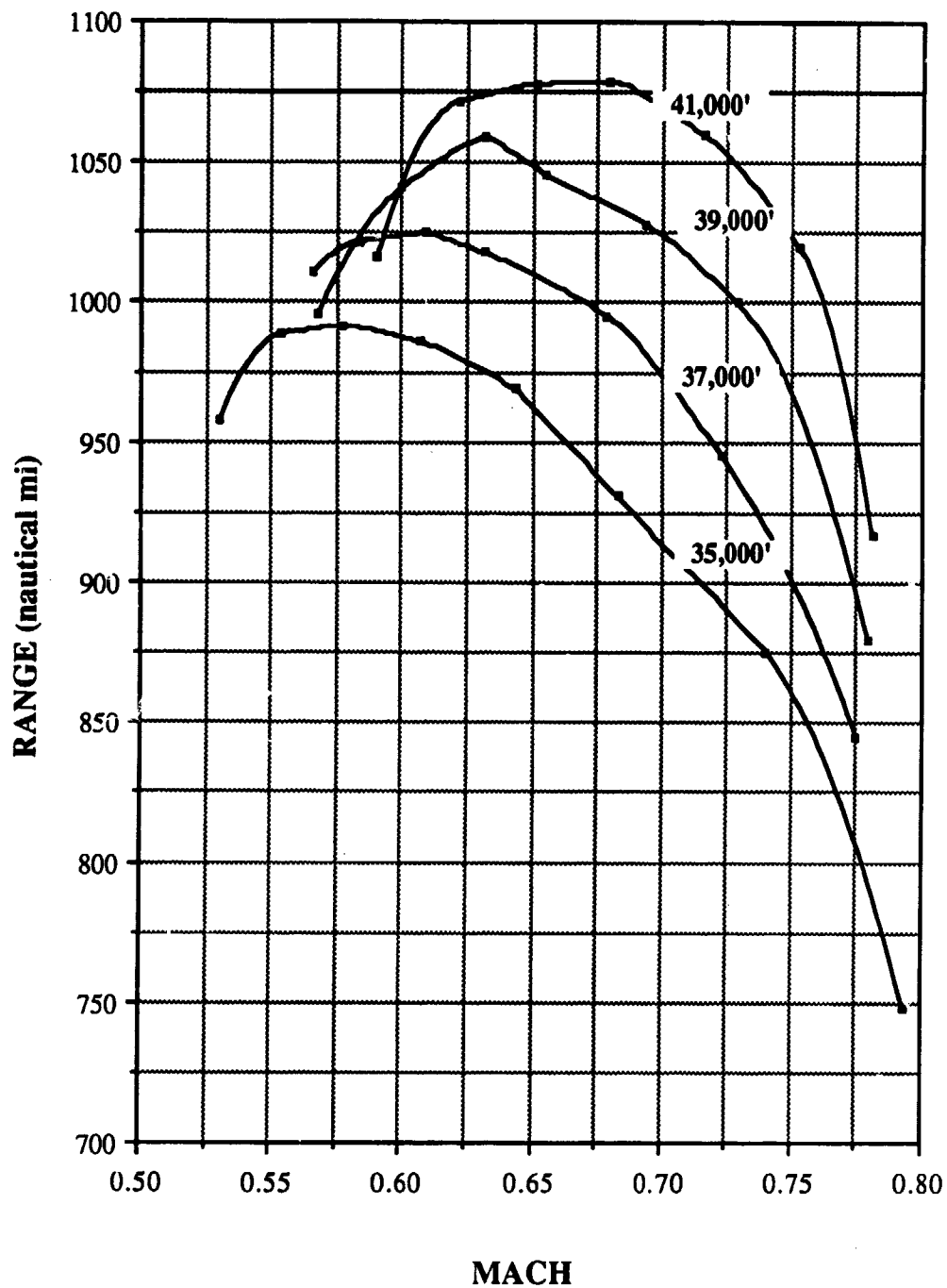
Figure 22. Best Range at Altitude (150,000 lbs)
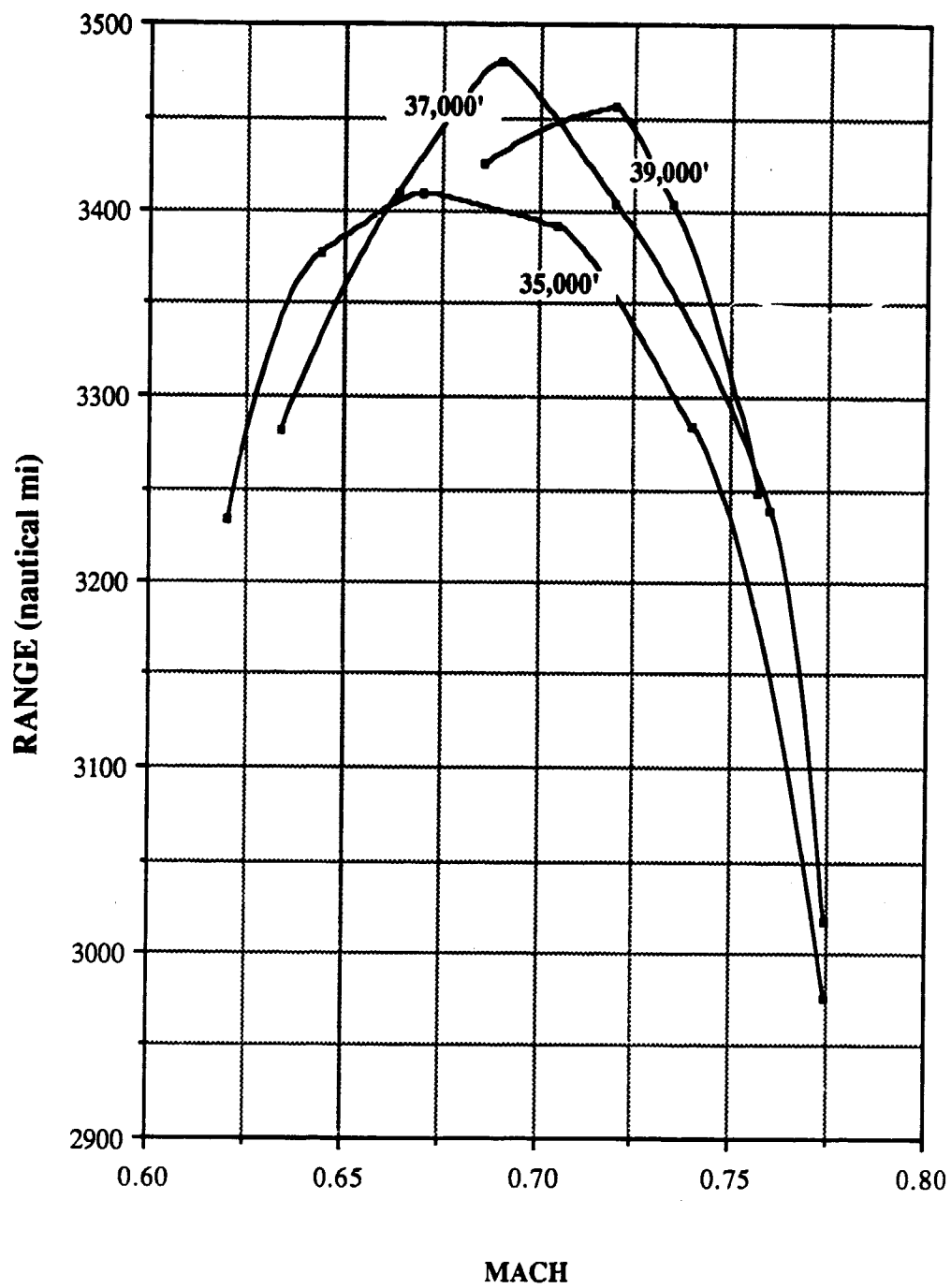
Figure 23. Best Range at Altitude (220,000 lbs)

ACFS MAXIMUM RANGE PERFORMANCE DATA

GROSS WEIGHT (lbs)	BEST CRUISE MACH	ABSOLUTE RANGE (naut. mi.)	BEST ALTITUDE (ft)	ACTUAL RANGE (naut. mi.)
150000	0.68	1080	41000	810
165000	0.69	1604	41000	1203
185000	0.7	2308	41000	1713
200,000	0.7	2804	39000	2103
220000	0.69	3480	37000	2610

Figure 24. ACFS Range Performance Data

150,000 to 220,000 pounds. This figure also illustrates that the best cruise Mach number is relatively constant throughout the range of gross weights.

The absolute range shown in Figure 24 is the value produced by Breguet's range equation, which neglects any fuel consumed during climb or descent and assumes that all fuel onboard was burned at altitude. In order to arrive at a more realistic number, the actual range is defined as the range from take-off to landing, with the following assumptions: 10% of the fuel was used for taxi, take-off, and climb to altitude; 5% for enroute descent, approach, and landing; and 10% in reserve for enroute delays and proceeding to an alternate airfield.

VI. APPROACH AND LANDING PERFORMANCE

A. HIGH LIFT DEVICE THEORY

In order to increase the lift coefficient of a wing, the circulation of the air around the wing must be increased, or the airflow separation on top of the wing must be delayed to prevent an early stall. The circulation may be increased by both increasing the wing angle of attack and increasing the camber in the region of the trailing edge of the wing. A trailing edge flap effectively increases the airfoil camber and increases the circulation, thus resulting in an increase in C_L. Leading edge slats are commonly used in conjunction with trailing edge flaps to delay airflow separation. [Ref. 9]

The ACFS employs multiple-slotted fowler flaps and extendable leading edge slats. Slotted fowler flaps provide slots between the main portion of the wing and the deflected flap section. The slots provide a form of boundary-layer control by ducting high-energy air from the lower surface to the upper surface and directing this air in such a manner as to delay flow separation over the flap. In addition, the flap surfaces move backward as well as downward when deployed. This aft movement results in an effective increase in total wing area. In addition to reducing flow

65

separation, the leading edge slats help to counter the pitching moment effects of the large trailing edge flaps.

The ACFS approach configuration lift curve (Figure 4) clearly demonstrates that increased flap deflection increases the maximum lift coefficient. However, increased flap deflection also results in an increase in the drag coefficient. In the approach configuration, an increase in drag is desirable since it acts to reduce the approach speed. This increase in drag also has the negative effect of increasing the thrust required for a wave-off or go-around procedure, in addition to severely limiting the single engine capability in the approach configuration.

Small initial deflections of fowler flaps cause noticeable changes in the maximum c_L without large changes in C_D. As the flap deflection increases beyond 30° to 35°, the rate of increase in C_D will exceed that of C_L. For most aircraft similarly configured, the first fifty percent of flap deflection causes more than half of the total change in the maximum C_L, while the last fifty percent in flap deflection causes more than half of the total change in C_D [Ref. 2]. Figures 4 and 25 clearly point out this fact in the case of the ACFS. The maximum lift coefficient for the 40° flap configuration is approximately 7 percent higher than that for 27° flaps. However, the lift to drag ratio, at the same angle of attack, for 40° flaps is approximately 18 percent less than that for 27° flaps. The 40° flap

66
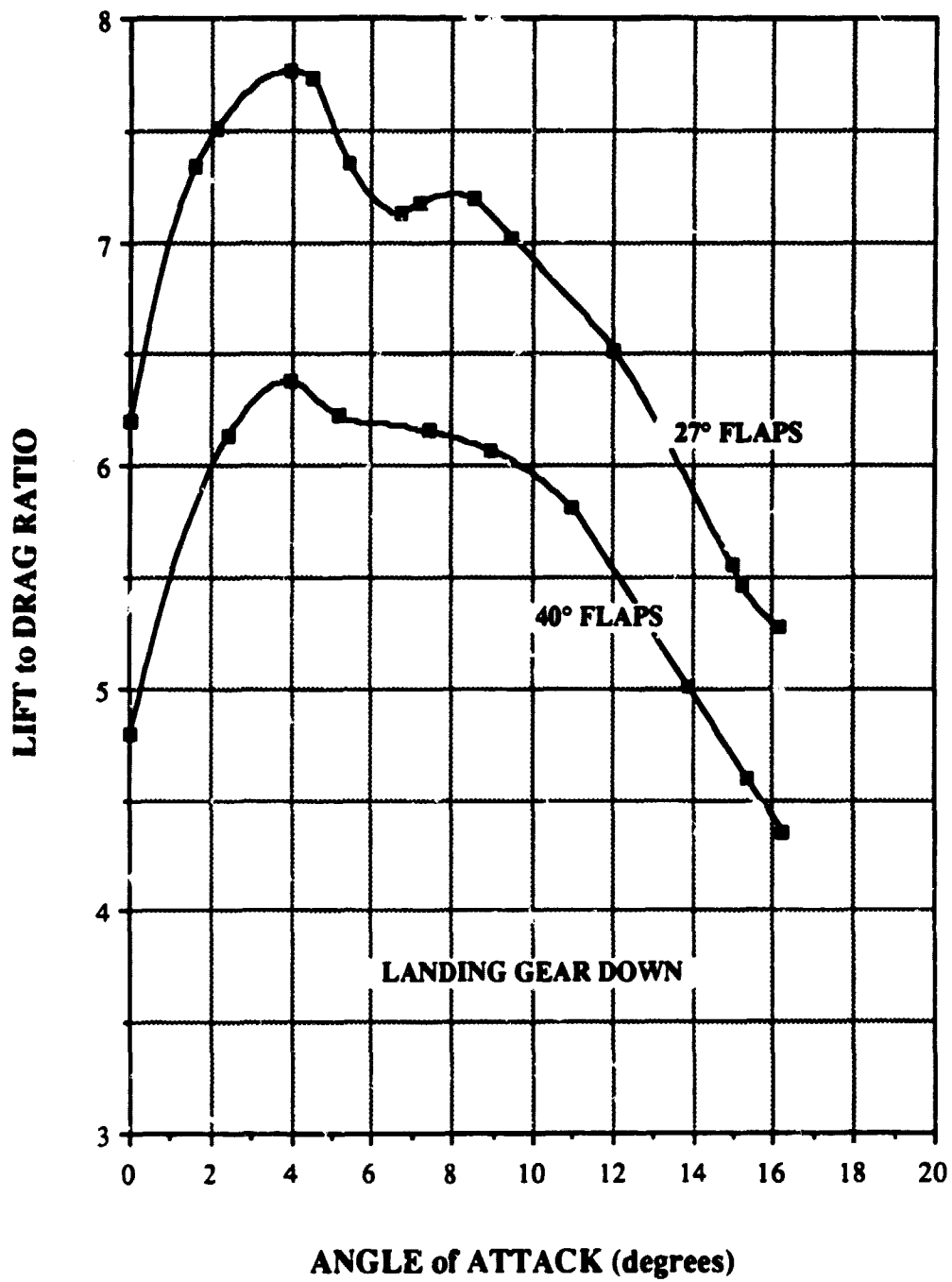
Figure 25. Approach Configuration Lift to Drag Ratios

configuration may produce a higher lift coefficient, but the penalty of the dramatic increase in drag is such that the lift to drag ratio, a measure of the efficiency of the flap configuration, is reduced to a value well below that for the 27° flap configuration.

B. TEST PROCEDURES AND RESULTS

The first step in the determination of approach and landing speeds for the ACFS is the establishment of the stall speeds. This procedure is described in detail in Chapter 2 of the report. The following transport aircraft criteria were applied to compute approach and landing speeds [Ref. 3]:

$$V_{app} = 1.3 \ V_S \tag{35}$$

and

$$V_{lnd} = 1.15 \ V_S \tag{36}$$

where

$$V_{app} = \text{approach speed}$$
$$V_{lnd} = \text{landing speed.}$$

Figure 26 contains the approach and landing speeds for flap settings of 27° and 40° for each ACFS gross weight selection.

68

ACFS APPROACH and LANDING SPEEDS
(sea level, standard day)

GROSS WT (lbs)	APPROACH SPEED		LANDING SPEED	
	27° FLAPS	40° FLAPS	27° FLAPS	40° FLAPS
150,000	131	129	116	114
165,000	138	134	122	118
185,000	146	142	129	123
200,000	151	148	133	131
220,000	159	155	140	137

Figure 26. ACFS Approach and Landing Speeds

69

VII. CONCLUSIONS AND RECOMMENDATIONS

The ACFS is a full-mission flight simulator which provides an excellent platform in which emerging flight systems and aircrew performance can be critically evaluated. As such, the aerodynamic performance model of the ACFS realistically represents that of current day, medium range transport aircraft. There are, however, two areas which should be modified in order to more closely model the projected capabilities of the 1995 transport aircraft that the simulator was designed to represent. These two areas are the lift characteristics in the approach configuration, and the engine static thrust available and corresponding thrust lapse rate.

Figure 27 [Ref. 10] shows the maximum lift capability (as represented by $C_{L\ max}$) of selected transport aircraft in the approach configuration through the year 1975. Due to advances in both trailing edge and leading edge high lift devices, the $C_{L\ max}$ has steadily risen to values exceeding 3.0. During the stall tests conducted in the ACFS, the value of $C_{L\ max}$ at the 40° flap configuration was found to be 2.08. A comparison of the lift capability of the ACFS with that of today's newest medium range transports (Figure 28) indicates that the high lift devices on the ACFS are not as effective as those currently employed on other similar

70
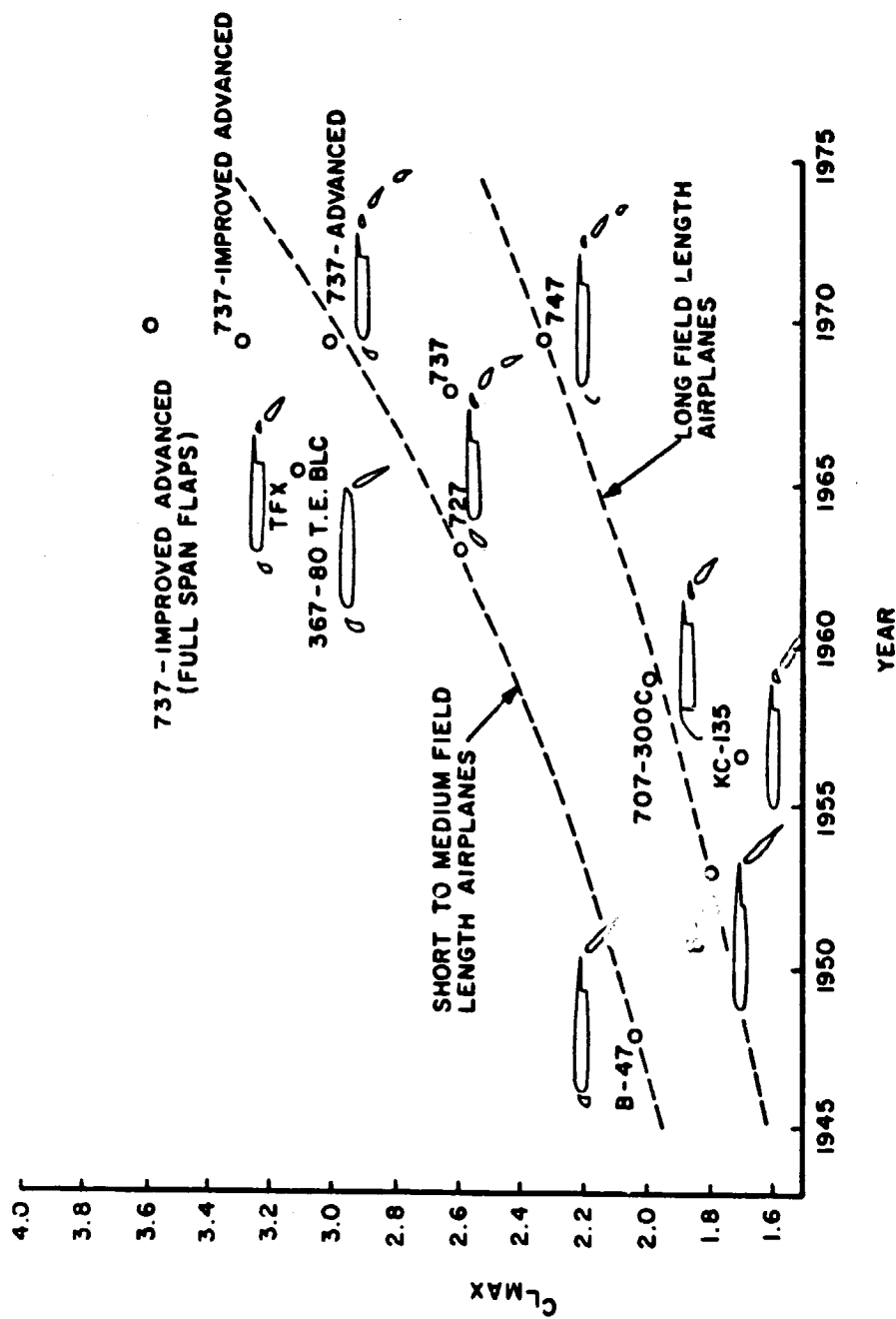
Figure 27.   Maximum Lift Capability of Selected Transport Aircraft

ACFS LIFT COMPARISON (Approach Configuration)	
AIRCRAFT TYPE	**MAXIMUM COEFFICIENT of LIFT**
ACFS	2.08
B-757	2.85
B-737-200	2.67
DC-10	2.87
A300	3.03
A310	3.12

Figure 28.   ACFS Lift Comparison

aircraft [Ref. 11]. A review of equation (1) indicates that the stall speed is indirectly proportional to the value of $C_{L\ max}$. A higher value of $C_{L\ max}$ for the ACFS would decrease the stall speed, and in turn lower the take-off, approach and landing speeds. It is recommended that the portion of the aerodynamic software model of the ACFS dealing with the leading and trailing edge devices be investigated to determine if higher values of $C_{L\ max}$ can be obtained in the approach configuration.

The ACFS take-off performance tests produced extremely short take-off roll distances, indicative of an excess amount of thrust available at sea level. At the maximum gross take-off weight of 220,000 pounds (on a standard day at sea level), the ACFS has a take-off roll of 3695 feet. By comparison, the Boeing 757 at the same weight and conditions has a take-off roll of 5600 feet [Ref. 11]. The thrust-to-weight ratios for the two aircraft at that weight are .38 and .34, respectively. It would appear that the obvious solution to bring the propulsion model of the ACFS more in line with current transport aircraft is to simply reduce the static thrust available. However, a review of the climb performance test results indicates that the thrust available at higher altitudes, where this type of aircraft is designed to operate, is not overly excessive, as indicated by a maximum rate of climb potential of 600 ft/min for a 185,000 pound aircraft at 41,000 feet.

Prior to the arrival of the high bypass turbofan engine, aircraft powered by conventional turbojet engines and designed for long range operations were confronted with the situation described above. In order to provide for adequate thrust available at altitude, the aircraft was overpowered on the ground, and was often required to take-off at a reduced power setting so as not to exceed engine RPM and temperature limits. Today, because of the dominant concern for efficient fuel consumption in transport aircraft, the optimum design favors the use of a turbofan engine with a high bypass ratio and a low fan pressure ratio. [Ref. 12]

In Reference 13, a method for estimating the variation of thrust available with Mach number and altitude is offered in the form of an algebraic equation that has been extrapolated from both existing data of published engine performance curves and predicted data based on future engine advances:

$$\alpha = [.568 + .25(1.2-M)^3] \sigma^{.6} \qquad (37)$$

where

α = engine thrust lapse rate

M = Mach number

σ = density ratio.

Equation (37) is based on the expected performance of high bypass turbofan engines (operating at a Mach number less than .9) in the year 1990 and beyond. Figure 29 presents a comparison between the actual thrust available for the ACFS (as a function of altitude) and the proposed thrust, computed with the aid of equation (37). Both thrust models have a static sea level thrust of 83,000 pounds; however, the proposed thrust available at altitude, ac a constant Mach number, is significantly higher than the actual ACFS thrust available. This is due to the optimization of several engine design parameters, such as bypass ratio, fan pressure ratio, and overall pressure ratio.

It is recommended that a review of the current ACFS propulsion model be conducted for the purpose of optimizing the thrust available. A reduction in static sea level thrust, coupled with a modification in the thrust lapse rate, will reduce both the weight of the engine and its thrust specific fuel consumption, thereby increasing the overall range of the aircraft.
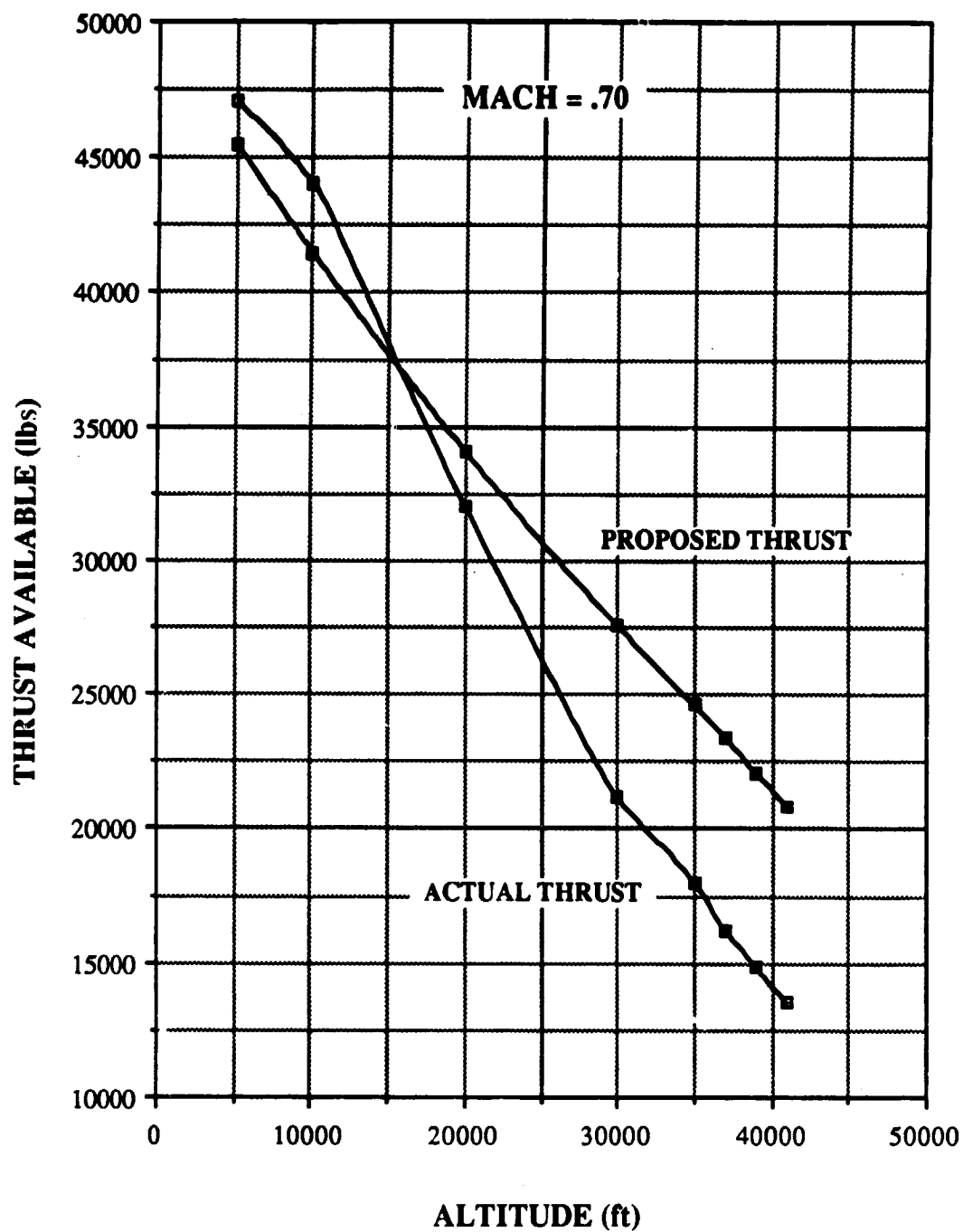
Figure 29. ACFS Thrust Lapse Rate Comparison

ACFS DESIGN CHARACTERISTICS

ACFS PERFORMANCE COMPARISON with BOEING 757 and AIRBUS 320 (sea level, standard day)			
	ACFS	B-757	A320
WING SPAN (ft)	139.7	124.7	111.3
ASPECT RATIO	9.00	7.77	9.39
FUSELAGE LENGTH (ft)	161.3	155.3	123.3
WING AREA (sq ft)	2170	1994	1318
WING SWEEP (deg)	24	25	25
MAX. PASSENGERS	200	186	179
MAX. GROSS WEIGHT (lbs)	220,000	220,000	145,505
EMPTY WEIGHT (lbs)	121,662	126,630	83,300
MAX. ZERO FUEL WT. (lbs)	177,500	184,000	125,665
WING LOADING (psf)	101.4	110.4	110.4
THRUST to WEIGHT RATIO	0.38	0.34	0.323
TOTAL THRUST (lbs)	83,700	74,800	47,000
MAX. FUEL (lbs)	42,500	36,000	27,590
MAX. RANGE (naut mi)	2610	2390	1930

ACFS TAKE-OFF GROSS WEIGHT SELECTIONS
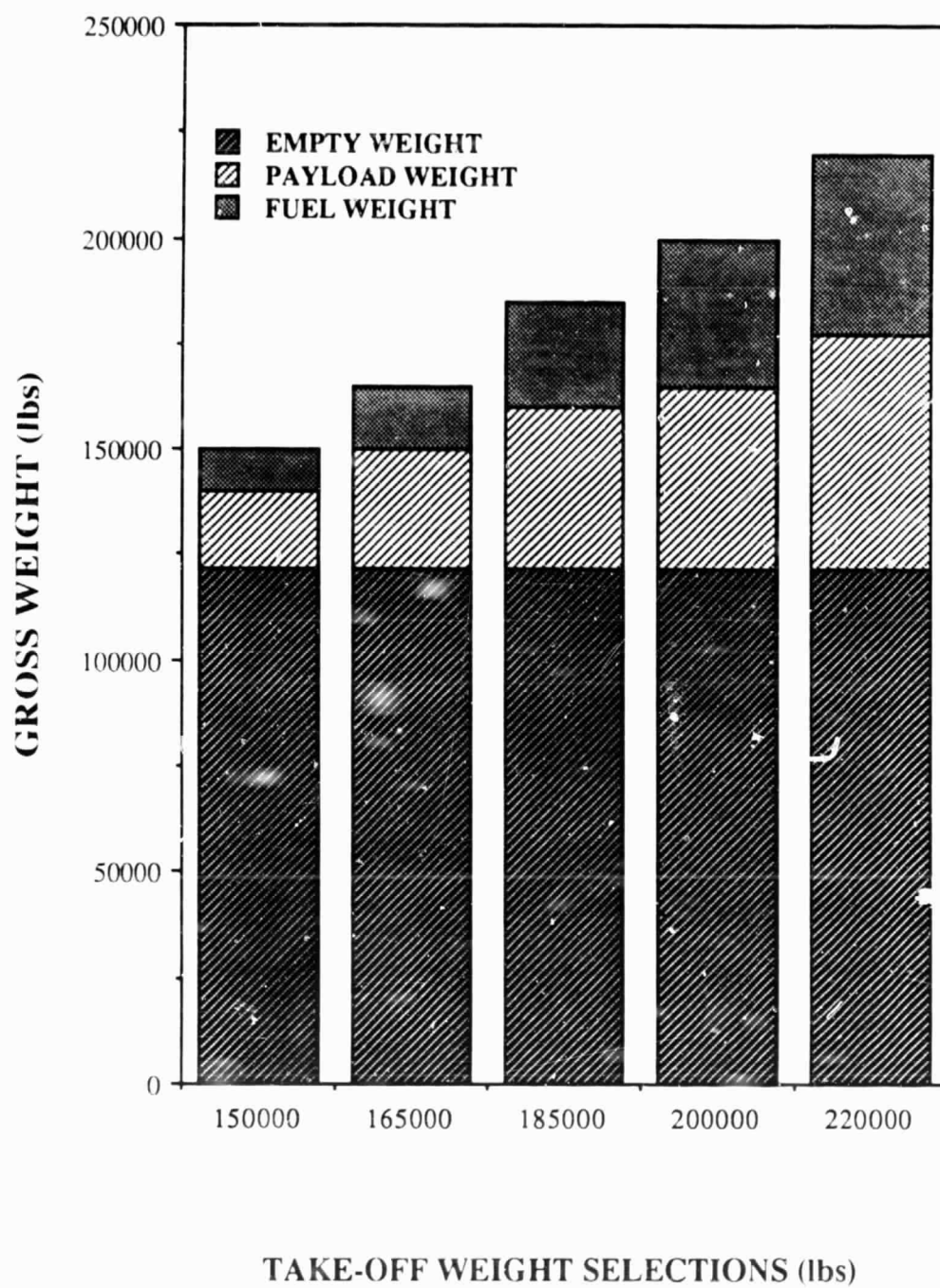
APPENDIX B

FORTRAN COMPUTER CODE

Several lines of code were inserted into the ACFS flight dynamics program in order to facilitate data reduction. The calculated variables used in the additional code are defined as follows:

TIME: Time in seconds; used primarily in the determination of take-off ground roll.

QBARS: Pressure force in pounds. It is the product of dynamic pressure (ENQ) and wing surface area (AOS).

DRAG: Drag force in pounds. It is the product of the total drag coefficient (AOCD) and QBARS. It is measured with respect to the stability axis.

PSUBS: Specific excess power in feet per second. It is used in the determination of rate of climb potential.

TAVG1: The average actual fuel flow per engine in pounds per hour. It is used in the calculation of thrust specific fuel flow (TSFF).

TAVG2: The average net thrust per engine in pounds. It is also used in the calculation of TSFF.

TSFF: Thrust specific fuel flow in pounds of fuel per second per pound of thrust. It is used in the calculation of the Breguet range equation.

TSFC: Thrust specific fuel consumption in pounds of fuel per hour per pound of thrust. It is a common measure of engine efficiency.

RHOS: The square root of the product of ambient air density (ENRHO) and wing surface area (AOS). It is a temporary storage variable used in the Brequet equation.

TAOCL: The square root of the lift coefficient (AOCL). It is also used in the Breguet equation.

WOWF: The difference between the square root of the actual gross weight and the square root of the zero fuel gross weight. It is also a temporary storage variable used in the Breguet equation.

RANGE: Range in nautical miles. It is the solution of the Breguet equation, and is a prediction of the optimal range obtainable based on zero excess power and constant TSFF.

The actual calculations are accomplished within the program as follows:

$$TIME = TIME + QESIK$$

where:

QESIK is the frame time constant in seconds

$$QBARS = ENQ * AOS$$

where:

ENQ is the dynamic pressure in pounds per square foot.

AOS is the wing surface area in square feet.

$$DRAG = AOCD * QBARS$$

$$PSUBS = ((PREXFOR * FDCALP - DRAG) * FDTAS)/WRGRWT$$

where:

PREXFOR is the total aircraft x-axis force due to thrust, in pounds. Since the engine incidence angle is zero, it is therefore the total thrust force.

FDCALP is the cosine of the angle of attack. It is used to obtain the thrust component parallel to the relative wind.

80

FDTAS is the aircraft true airspeed in feet per second.

WRGRWT is the aircraft total gross weight in pounds.

TAVG1 = (PRFF(1) + PRFF(2)) / 2.0

where:

PRFF(i) is the actual fuel flow in pounds of the ith engine.

TAVG(2) = (PRTHRUS(1) + PRTHRUS(2))/2.0

where:

PRTHRUS(i) is the net thrust in pounds of the ith engine.

TSFF = TAVG1/3600.0/TAVG2

TSFC = TAVG1/TAVG2

RHOS = ASQRT (ENRHO * AOS)

TAOCL = ASQRT (AOCL)

WOWF = ASQRT (WTGRWT) -
                    ASQRT (WTGRWT - WTFULWT)

where:

WTFULWT is the remaining fuel weight in pou..ds.

RANGE = (2.828 * TAOCL * WOWF)/
                (TSFF * AOCD * RHOS * 6080.2)

81

ACFS PERFORMANCE CHARTS

ACFS STALL AIRSPEEDS APPROACH CONFIGURATION				
GROSS WEIGHT (lbs)	FLAP SETTING			
	40°	27°	5°	0°
	KNOTS (IAS)			
150000	99	101	123	128
165000	103	106	129	135
185000	109	112	137	143
200000	114	116	142	149
220000	119	122	149	156

ACFS STALL AIRSPEEDS CLEAN CONFIGURATION				
GROSS WEIGHT (lbs)	ALTITUDE			
	5000'	10,000'	20,000'	30,000'
	KNOTS (IAS)			
150000	128	129	130	132
165000	135	135	136	138
185000	143	144	145	146
200000	149	147	150	152
220000	156	156	158	160

ACFS TAKE-OFF PERFORMANCE DATA

PRESSURE ALTITUDE: sea level

TRiM : zero

GEAR: down
FLAPS: T/O

TAKE-OFF GROSS WT (lbs)	OUTSIDE AIR TEMPERATURE (°C)								
	-15° to 4°			5° to 25°			26° to 46°		
	Vr	V2	T/O DiST	Vr	V2	T/O DIST	Vr	V2	T/O DIST
150,000	116	121	1403	116	121	1512	117	122	1611
165,000	121	127	1775	121	127	1838	122	128	1918
185,000	128	135	2355	128	135	2391	129	136	2490
200,000	133	139	2848	133	139	2873	134	140	3072
220,000	140	147	3590	140	147	3695	141	148	4005

ACES TAKE-OFF PERFORMANCE DATA

PRESSURE ALTITUDE: 1000'

TRIM :	zero

GEAR:	down
FLAPS:	T/O

TAKE-OFF GROSS WT (lbs)	OUTSIDE AIR TEMPERATURE (°C)								
	-15° to 4°			5° to 25°			26° to 46°		
	Vr	V2	T/O DIST	Vr	V2	T/O DIST	Vr	V2	T/O DIST
150,000	116	121	1531	116	121	1560	117	122	1596
165,000	121	127	1881	121	127	1934	122	128	1965
185,000	128	135	2441	128	135	2505	129	136	2573
200,000	133	139	2906	133	139	2988	134	140	3104
220,000	140	147	3625	140	147	3703	141	148	3931

84

ACFS TAKE-OFF PERFORMANCE DATA

PRESSURE ALTITUDE: 2000'

TRIM :	zero

GEAR:	down
FLAPS:	T/O

OUTSIDE AIR TEMPERATURE (°C)

TAKE-OFF GROSS WT (lbs)	-15° to 4°			5° to 25°			26° to 46°		
	Vr	V2	T/O DIST	Vr	V2	T/O DIST	Vr	V2	T/O DIST
150,000	116	121	1572	116	121	1602	117	122	1639
165,000	121	127	1941	121	127	19.8	122	128	2041
185,000	128	135	2508	128	135	2573	129	136	2643
200,000	133	139	2999	133	139	3071	134	140	3185
220,000	140	147	3726	140	147	3807	141	148	4043

ACES TAKE-OFF PERFORMANCE DATA

PRESSURE ALTITUDE: 3000'

TRIM :	zero

GEAR:	down
FLAPS:	T/O

TAKE-OFF GROSS WT (lbs)	OUTSIDE AIR TEMPERATURE (°C)								
	-15° to 4°			5° to 25°			26° to 46°		
	Vr	V2	T/O DIST	Vr	V2	T/O DIST	Vr	V2	T/O DIST
150,000	116	121	1614	116	121	1645	117	122	1682
165,000	121	127	1998	121	127	2041	122	128	2075
185,000	128	135	2576	128	135	2643	129	136	2715
200,000	133	139	3086	133	139	3156	134	140	3283
220,000	140	147	3830	140	147	3914	141	148	4157

ACES TAKE-OFF PERFORMANCE DATA

PRESSURE ALTITUDE: 4000'

TRIM : zero

GEAR: down
FLAPS: T/O

TAKE-OFF GROSS WT (lbs)	OUTSIDE AIR TEMPERATURE (°C)											
	-15° to 4°			5° to 25°			26° to 46°		
	Vr	V2	T/O DIST	Vr	V2	T/O DIST	Vr	V2	T/O DIST
150,000	116	121	1557	116	121	1689	117	122	1727
165,000	121	127	2042	121	127	2093	122	128	2132
185,000	128	135	2646	128	135	2716	129	136	2790
200,000	133	139	3161	133	139	3241	134	140	3376
220,000	140	147	3938	140	147	4024	141	148	4275

87

ACFS TAKE-OFF PERFORMANCE DATA

PRESSURE ALTITUDE: 5000'

TRIM :	zero

GEAR:	down
FLAPS:	T/O

TAKE-OFF GROSS WT (lbs)	OUTSIDE AIR TEMPERATURE (°C)								
	-15° to 4°			5° to 25°			26° to 46°		
	Vr	V2	T/O DIST	Vr	V2	T/O DIST	Vr	V2	T/O DIST
150,000	116	121	1701	116	121	1734	117	122	1774
165,000	121	127	2097	121	127	2153	122	128	2190
185,000	128	135	2719	128	135	2790	129	136	2867
200,000	133	139	3249	133	139	3336	134	140	3471
220,000	140	147	4049	140	147	4137	141	148	4397

88

RATE of CLIMB POTENTIAL
Gross Weight: 185,000 lbs
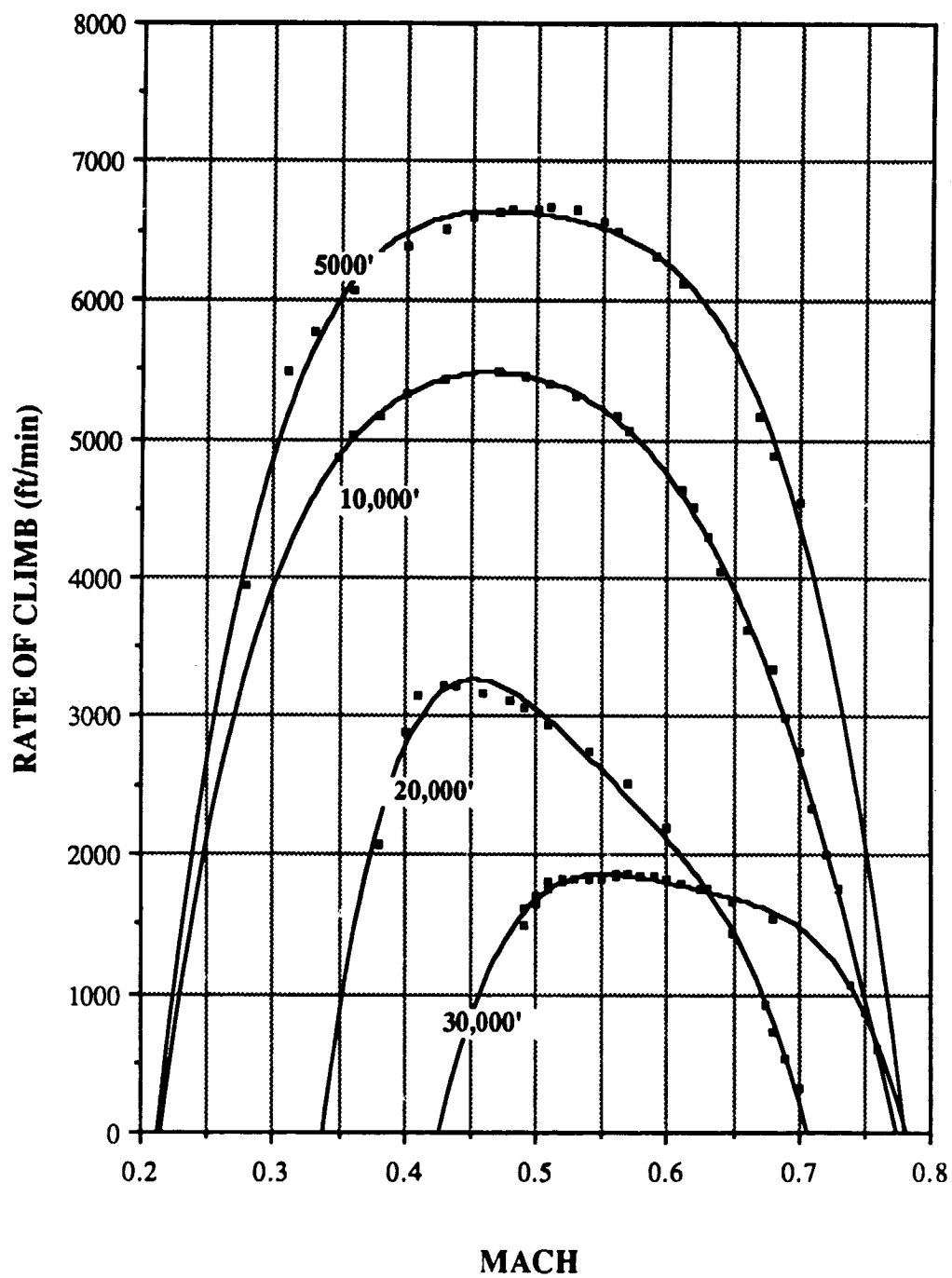
RATE of CLIMB POTENTIAL
Gross Weight: 185,000 lbs
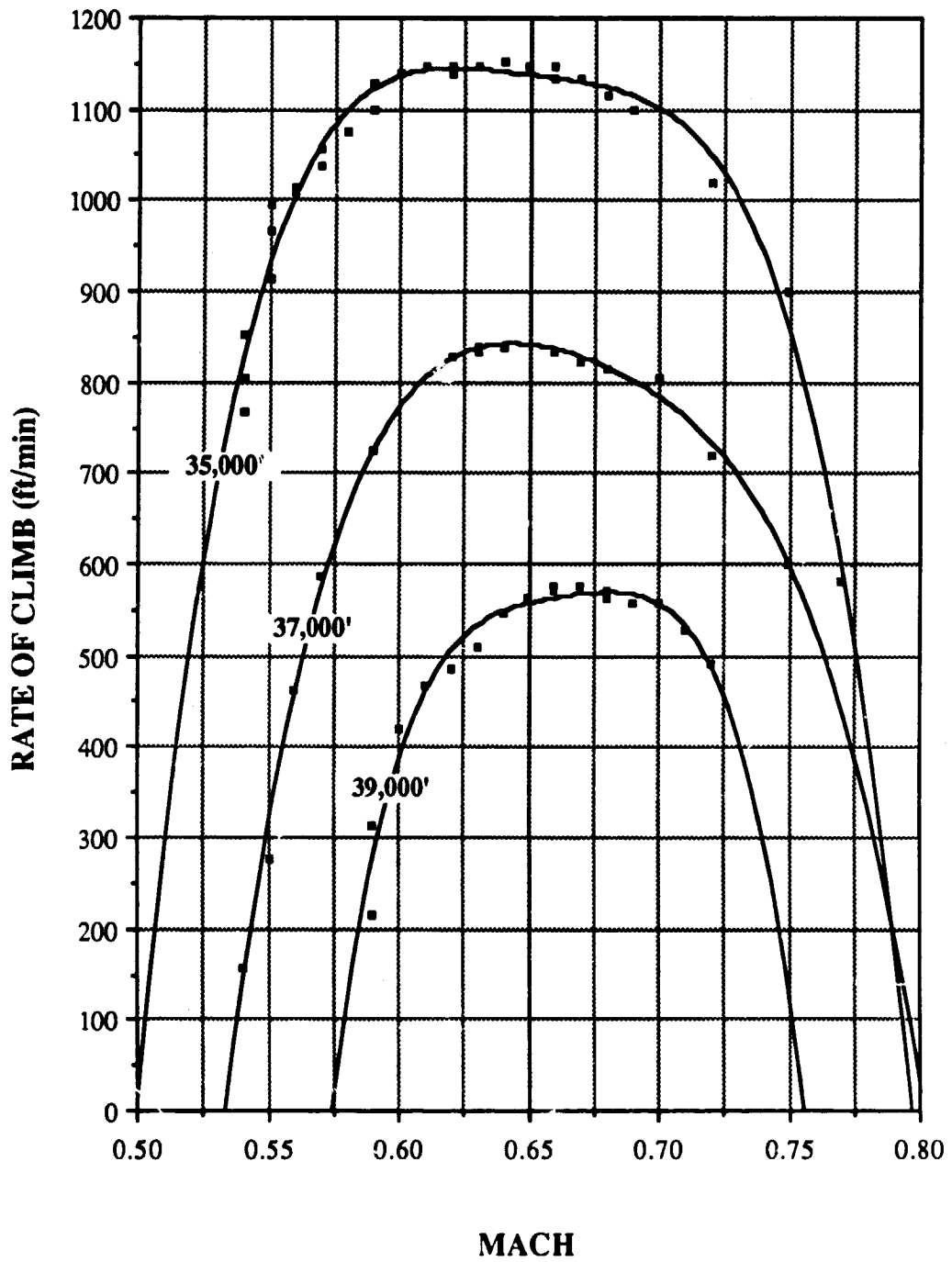
BEST RANGE at ALTITUDE

Gross Weight: 150,000 lbs
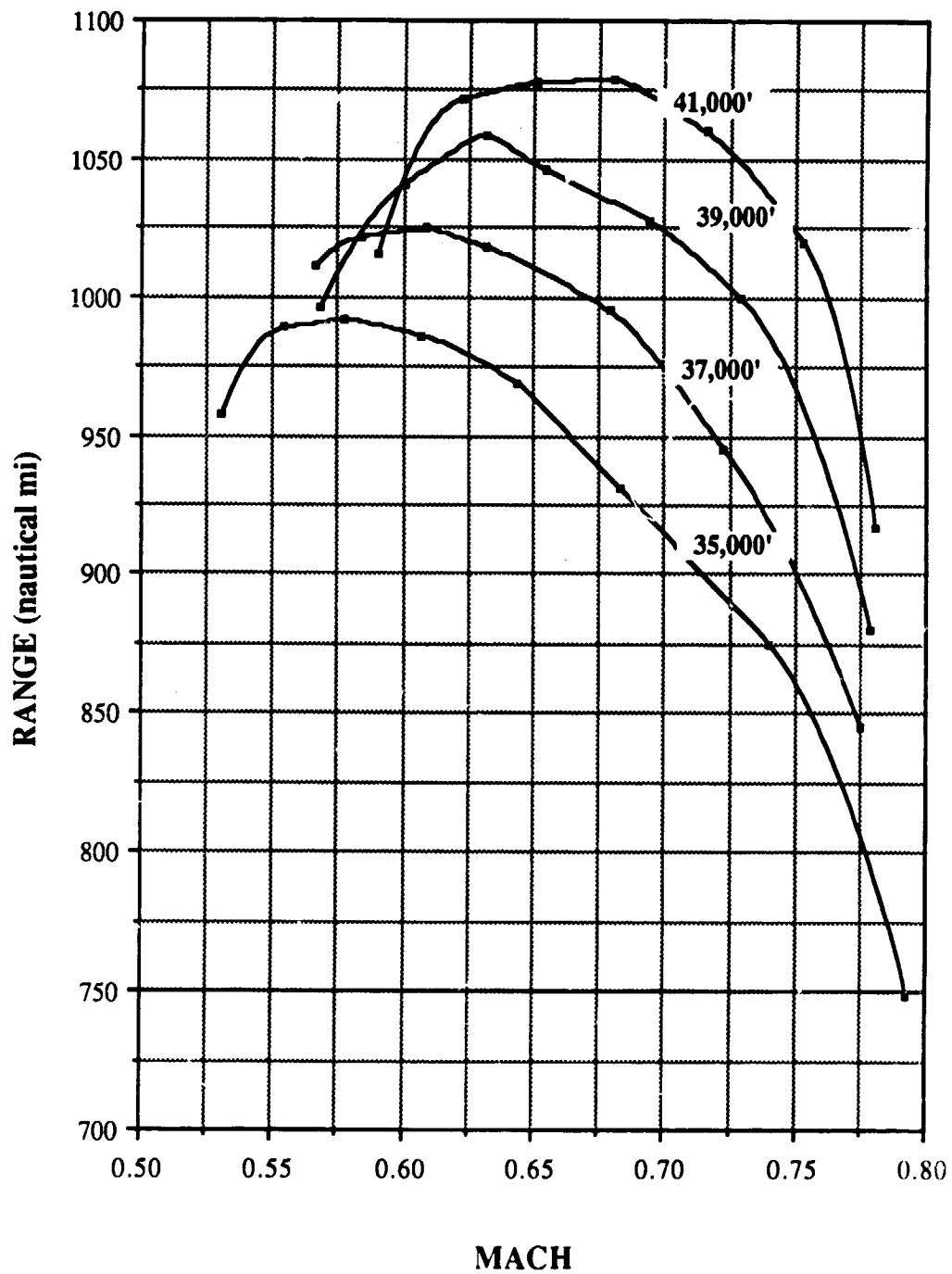
BEST RANGE at ALTITUDE

Gross Weight: 220,000 lbs

92
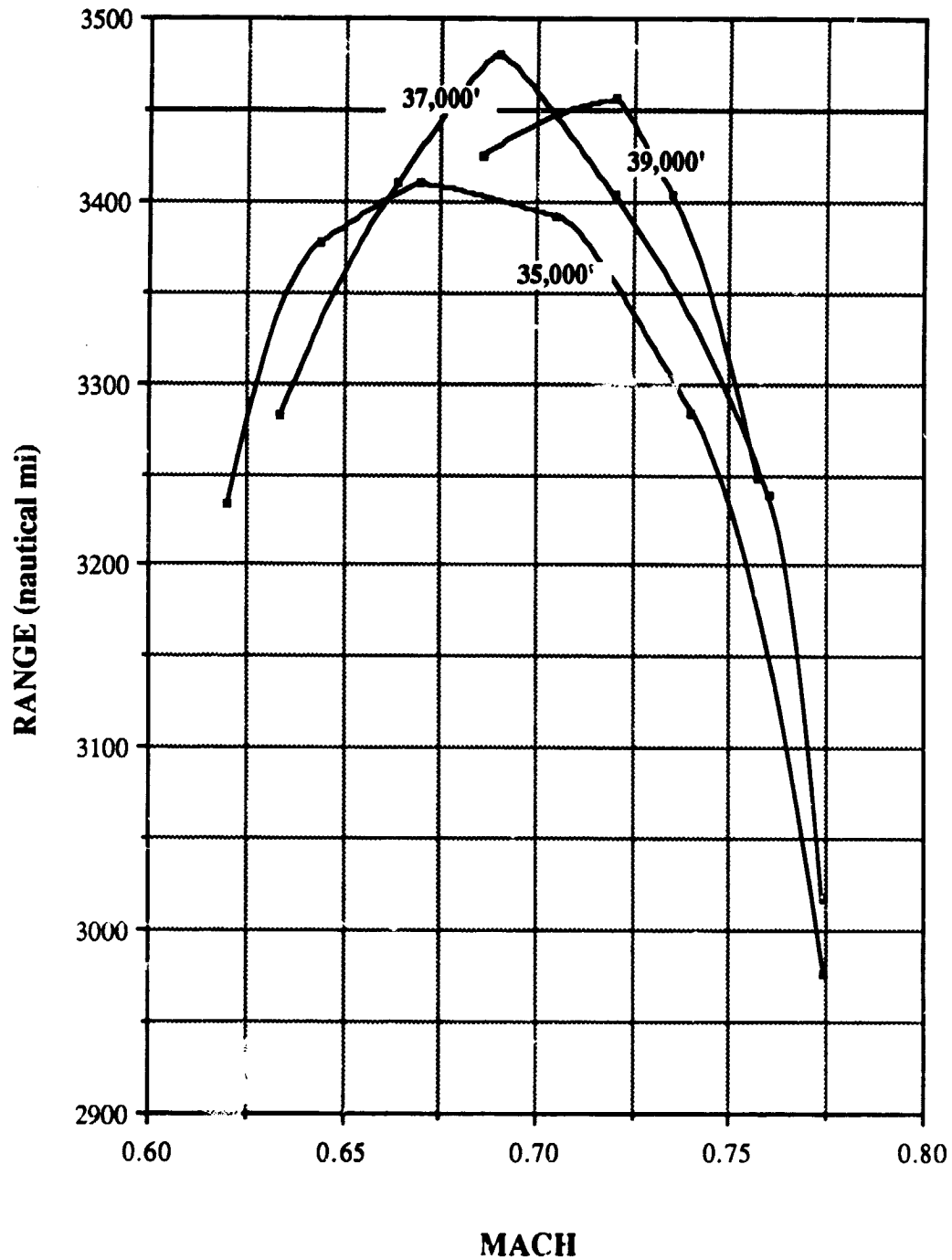
RATE of CLIMB POTENTIAL (41,000 ft)

BEST RANGE at ALTITUDE
Gross Weight: 185,000 lbs

Chart titled "BEST RANGE at ALTITUDE" with y-axis "RANGE (nautical mi)" ranging from 500 to 2250 and x-axis "MACH" ranging from 0.2 to 0.9. Curves labeled 5000', 10,000', 20,000', and 30,000'.
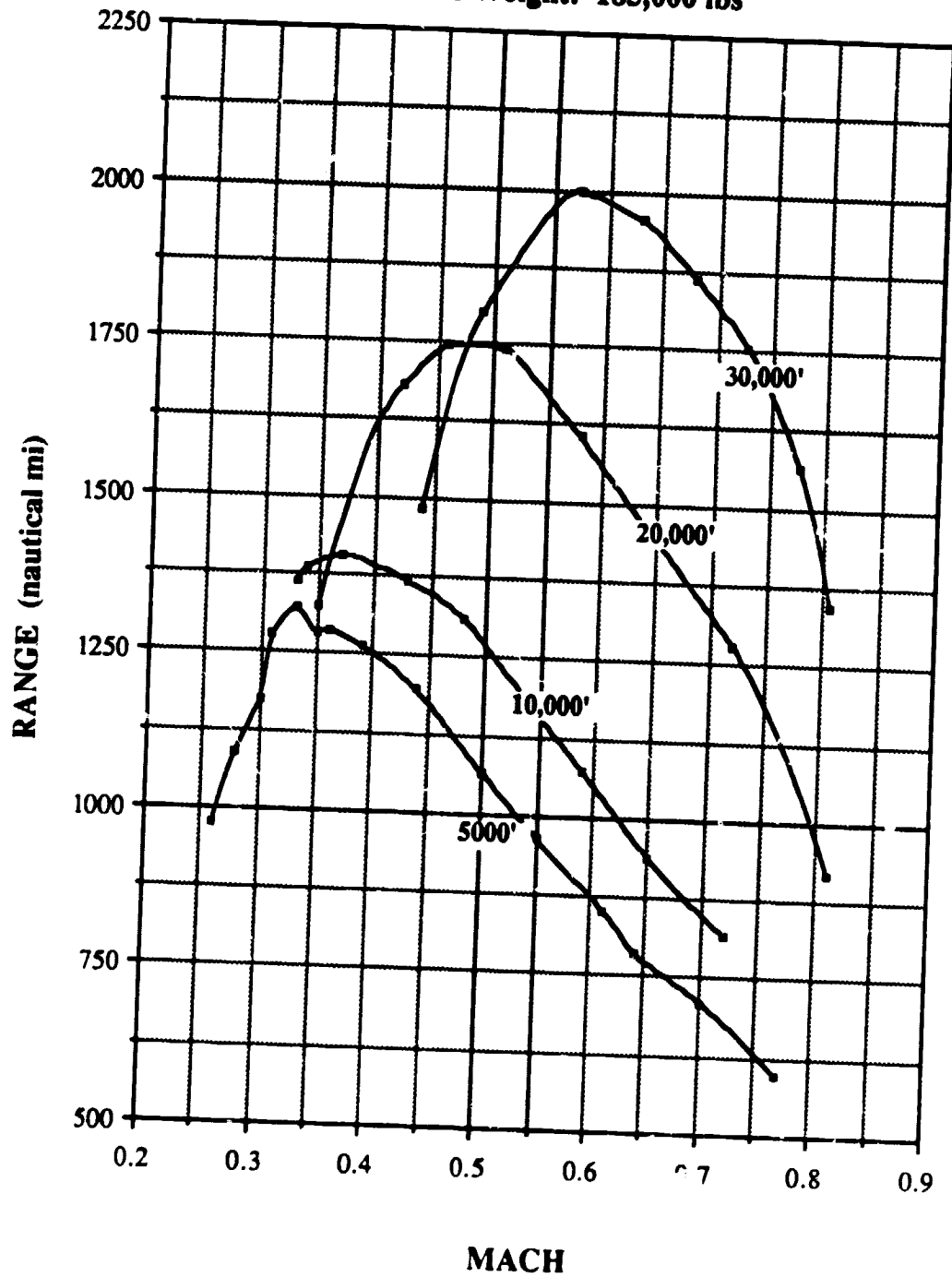
MACH

BEST RANGE at ALTITUDE

Gross Weight: 185,000 lbs
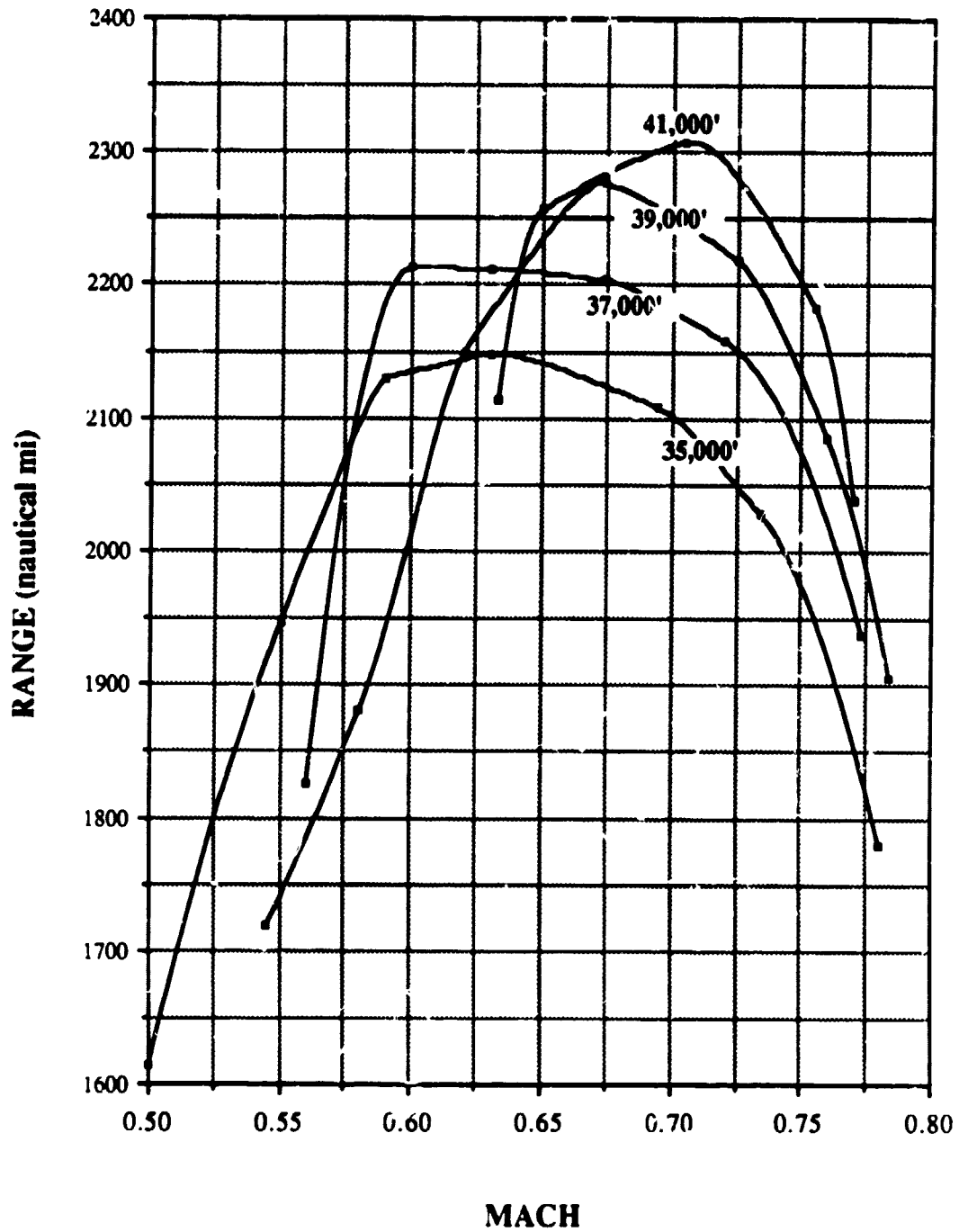
ACFS MAXIMUM RANGE PERFORMANCE DATA

GROSS WEIGHT (pounds)	BEST MACH	ABSOLUTE RANGE (naut. mi.)	BEST ALTITUDE (ft)	ACTUAL RANGE (naut. mi.)
150000	0.68	1080	41000	810
165000	0.69	1604	41000	1203
185000	0.7	2308	41000	1713
200,000	0.7	2804	39000	2103
220000	0.69	3480	37000	2610

ACFS APPROACH and LANDING SPEEDS
(sea level, standard day)

GROSS WT (lbs)	APPROACH SPEED		LANDING SPEED	
	27° FLAPS	40° FLAPS	27° FLAPS	40° FLAPS
150,000	131	129	116	114
165,000	138	134	122	118
185,000	146	142	129	123
200,000	151	148	133	131
220,000	159	155	140	137

ACFS PERFORMANCE TEST DATA

TAKE-OFF ROLL ACCELERATION
GROSS WEIGHT: 150,000 lbs
PRESSURE ALT: sea level

TEMP: -5°C		TEMP: 15°C		TEMP: 35°C	
VEL (ft/sec)	TIME (sec)	VEL (ft/sec)	TIME (sec)	VEL (ft/sec)	TIME (sec)
0	0	0	0	0	0
107.76	6.8	89.72	6.1	82.3	5
155.05	10.2	146.88	9.9	129.19	8.2
192.02	13	185.72	13.2	179.24	11.9
229.79	16.2	217.98	15.9	215.35	14.8
255.09	18.6	250.16	18.4	249.21	17.9
276.71	21	278.36	20.7	272.76	20.3
295.15	23	301.77	22.9	294.9	22.7

TAKE-OFF ROLL ACCELERATION
GROSS WEIGHT: 185,000 lbs
PRESSURE ALT: sea level

TEMP: -5°C		TEMP: 15°C		TEMP: 35°C	
VEL (ft/sec)	TIME (sec)	VEL (ft/sec)	TIME (sec)	VEL (ft/sec)	TIME (sec)
0	0	0	0	0	0
42.9	3.9	35.71	3.8	44.9	5
77.9	6.4	67.24	6.2	81.4	8
108.1	8.9	105.7	9.4	109.8	10.4
138.7	11.4	131.1	11.5	140	13
168.9	14.1	174.1	15.4	167	15.6
204	17.5	200.2	17.9	190	18
235.9	20.8	224.6	20.4	214	20.4
255.9	23.1	243.7	22.6	231.9	22.4
275.3	25.5	265	25.1	256.4	25.4
298.8	28	292.5	28.7	277.8	28.2

TAKE-OFF ROLL ACCELERATION
GROSS WEIGHT: 220,000 lbs
PRESSURE ALT: sea level

TEMP: -5°C		TEMP: 15°C		TEMP: 35°C	
VEL (ft/sec)	TIME (sec)	VEL (ft/sec)	TIME (sec)	VEL (ft/sec)	TIME (sec)
0	0	0	0	0	0
28.5	3.2	26.4	3.4	28.4	3.6
71.1	7.1	73.1	7.8	65.2	7.4
101.7	10	105.1	11	101.3	11.3
134.6	13.4	131.9	13.7	133.1	14.9
171.3	17.4	168.7	18	168.1	19.1
203.9	21.3	207.6	22.7	203	23.8
235.3	25.4	236.8	27	234.6	28.5
265.7	30	265.5	31.2	264.7	33.6

APPROACH CONFIGURATION STALL DATA
ALTITUDE: 5000'

FLAP POSITION

27°		40°		5°		0°	
Cl	AOA	Cl	AOA	Cl	AOA	Cl	AOA
0.93	1.6	1.105	2.43	0.788	3.45	0.685	3.167
0.983	2.11	1.271	3.97	0.885	4.5	0.775	4.25
1.18	3.99	1.387	5.2	0.926	5.15	0.834	5.06
1.23	4.5	1.6	7.44	1.03	6.53	0.908	6.08
1.32	5.43	1.73	8.99	1.12	7.645	1	7.34
1.44	6.72	1.885	10.95	1.19	8.86	1.044	7.95
1.48	7.18	2.05	13.91	1.276	10.39	1.088	8.8
1.59	8.51	2.105	15.37	1.343	11.58	1.15	10
1.66	9.47	2.106	16.24	1.255	16.25	1.174	10.5
1.87	12.04					1.233	12.24
1.963	14.99					1.118	13.85
1.967	15.24						
2.02	16.17						
1.97	16.38						

CLEAN CONFIGURATION STALL DATA
LANDING GEAR, FLAPS: UP

PRESSURE ALTITUDE

5000'		20,000'		30,000'		41,000'	
Cl	AOA	Cl	AOA	Cl	AOA	Cl	AOA
0.55	1.63	0.64	2.71	0.66	2.91	0.706	3.59
0.594	2.122	0.712	3.52	0.713	3.54	0.771	4.61
0.668	2.98	0.81	4.74	0.794	4.58	0.928	6.92
0.704	3.4	0.906	6.14	0.89	6	1.019	8.32
0.775	4.27	1.013	7.62	0.96	6.97	1.081	9.62
0.93	6.4	1.08	8.73	1.07	8.78	1.145	10.875
0.996	7.3	1.176	10.65	1.124	9.89	1.135	11.66
1.091	8.89	1.21	12.28	1.183	10.99		
1.216	11.33	1.2	12.67	1.18	12.64		
1.24	12.21	1.12	13.28				
1.1	14.475						

ACCELERATION RUN DATA
GROSS WEIGHT: 185,000 lbs

PRESSURE ALTITUDE

5000'		10,000'		20,000'		30,000'	
MACH	ROC	MACH	ROC	MACH	ROC	MACH	ROC
0.29	3948	0.35	4872	0.38	2074.2	0.475	1704
0.31	5478	0.36	5028	0.4	2886	0.505	1920
0.33	5778	0.38	5166	0.41	3144	0.555	2118
0.36	6078	0.4	5328	0.43	3216	0.58	2154
0.38	6240	0.43	5442	0.44	3213	0.6	2154
0.4	6396	0.47	5490	0.46	3168	0.62	2148
0.43	6522	0.49	5460	0.48	3120	0.65	2100
0.45	6600	0.51	5400	0.49	3060	0.675	2034
0.47	6642	0.53	5304	0.51	2946	0.53	2070
0.48	6660	0.55	5160	0.54	2751	0.705	1926
0.5	6660	0.57	5058	0.57	2517	0.73	1758
0.51	6678	0.61	4632	0.6	2190	0.75	1542
0.53	6648	0.62	4512	0.625	1752	0.775	1134
0.55	6564	0.63	4296	0.65	1428	0.794	702
0.56	6492	0.64	4056	0.675	918	0.806	84
0.59	6324	0.66	3624	0.68	726		
0.61	6120	0.68	3348	0.69	528		
0.67	5172	0.69	2988	0.7	324		
0.68	4884	0.7	2748				
0.7	4542	0.71	2328				
		0.72	2004				
		0.73	1758				

ACCELERATION RUN DATA
GROSS WEIGHT: 185,900 lbs

PRESSURE ALTITUDE

35,000'		37,000'		39,000'		41,000'	
MACH	ROC	MACH	ROC	MACH	ROC	MACH	ROC
0.54	768	0.54	156	0.59	216	0.65	465
0.54	804	0.55	276	0.59	312	0.655	504.6
0.54	852	0.56	462	0.6	420	0.66	513.6
0.55	912	0.57	588	0.61	468	0.68	587.4
0.55	966	0.59	726	0.62	486	0.7	621
0.55	996	0.62	828	0.63	510	0.72	581.4
0.56	1008	0.63	834	0.64	546	0.74	557.4
0.56	1014	0.63	840	0.65	564	0.76	351
0.57	1038	0.64	840	0.66	570	0.77	199.8
0.57	1056	0.66	834	0.66	576		
0.58	1074	0.67	822	0.67	576		
0.59	1098	0.68	816	0.68	570		
0.59	1128	0.7	804	0.68	564		
0.6	1140	0.72	720	0.69	558		
0.6	1146	0.75	600	0.7	558		
0.62	1146			0.71	528		
0.63	1146			0.72	492		
0.64	1152						
0.65	1146						
0.66	1146						
0.67	1134						
0.68	1116						
0.69	1098						
0.72	1020						
0.75	900						
0.77	582						

ACCELERATION RUN DATA
PRESSURE ALTITUDE: 41,000'

GROSS WEIGHT (lbs)						
150,000		185,000		220,000	
MACH	ROC	MACH	ROC	MACH	ROC
0.568	681.6	0.65	465	0.685	424.2
0.605	1165.2	0.655	504.6	0.699	468
0.64	1251	0.66	513.6	0.707	477.6
0.672	1301.4	0.68	587.4	0.718	457.8
0.696	1319.4	0.7	621	0.734	414
0.709	1308	0.72	581.4	0.747	393.6
		0.74	557.4	0.762	195.6
		0.76	351		
		0.77	199.8		

STABILIZED RUN DATA
GROSS WEIGHT: 185,000 lbs

PRESSURE ALTITUDE

5,000'		10,000'		20,000'		30,000'	
MACH	RANGE	MACH	RANGE	MACH	RANGE	MACH	RANGE
0.26	978	0.33	1363	0.35	1325	0.44	1482
0.28	1090	0.34	1388	0.42	1680	0.49	1801
0.3	1174	0.37	1407	0.46	1748	0.574	2000
0.31	1280	0.43	1367	0.51	1744	0.63	1956
0.33	1320	0.48	1311	0.58	1606	0.68	1864
0.35	1283	0.54	1180	0.64	1465	0.727	1753
0.36	1287	0.59	1072	0.72	1279	0.775	1564
0.39	1262	0.65	939	0.81	917	0.805	1345
0.44	1195	0.72	818				
0.5	1067						
0.55	966						
0.61	853						
0.64	786						
0.7	711						
0.77	595						

STABILIZED RUN DATA
GROSS WEIGHT: 185,000 lbs

PRESSURE ALTITUDE

35,000'		37,000'		39,000'		41,000'	
MACH	RANGE	MACH	RANGE	MACH	RANGE	MACH	RANGE
0.5	1615	0.56	1825	0.545	1719	0.633	2114
0.55	1947	0.6	2213	0.58	1880	0.65	2257
0.59	2130	0.63	2212	0.62	2149	0.705	2308
0.63	2148	0.674	2204	0.674	2277	0.755	2183
0.695	2108	0.72	2158	0.725	2219	0.77	2039
0.734	2029	0.770	1937	0.76	2085		
0.78	1780			0.784	1905		

STABILIZED RUN DATA
GROSS WEIGHT: 150,000 lbs

PRESSURE ALTITUDE							
35,000'		37,000'		39,000'		41,000'	
MACH	RANGE	MACH	RANGE	MACH	RANGE	MACH	RANGE
0.53	958	0.566	1011	0.568	996	0.59	1016
0.554	989	0.584	1022	0.6	1041	0.622	1072
0.577	992	0.609	1025	0.632	1059	0.651	1078
0.607	986	0.632	1018	0.655	1046	0.68	1079
0.644	969	0.679	995	0.694	1028	0.716	1060
0.683	931	0.723	945	0.729	1000	0.753	1020
0.74	875	0.775	845	0.779	880	0.781	917
0.793	748						

STABILIZED RUN DATA
GROSS WEIGHT: 220,000 lbs

PRESSURE ALTITUDE

35,000'		37,000'		39,000'	
MACH	RANGE	MACH	RANGE	MACH	RANGE
0.57	2635	0.634	3282	0.686	3425
0.62	3233	0.664	3410	0.72	3456
0.644	3378	0.69	3480	0.735	3404
0.67	3410	0.72	3404	0.757	3248
0.705	3392	0.76	3239		
0.74	3284	0.774	3017		
0.774	2976				

109

LIST OF REFERENCES

1. National Aeronautics and Space Administration Contractor Report 166068, Crew Systems and Flight Station Concepts for a 1995 Transport Aircraft, by George A. Sexton, 1 April 1983.

2. Hurt, H. H., Aerodynamics for Naval Aviators, Office of the Chief of Naval Operations, 1965.

3. Airworthiness Standards: Part 25--Transport Category Aircraft, Federal Aviation Regulations, Department of Transportation, U.S. Government Printing Office, Washington, D.C., December 1969.

4. U.S. Air Force Test Pilot School, Performance Flight Testing Theory, January 1973.

5. Layton, Donald M., Airplane Performance, Matrix Publishers, Inc. (To Be Published).

6. Lan, C. E. and Roskam, J., Airplane Aerodynamics and Performance, Roskam Aviation and Engineering Corp., 1981.

7. Jet Transport Performance Methods, D6-1420, The Boeing Co., 1969.

8. U.S. Naval Test Pilot School, Fixed Wing Performance, Theory, and Flight Test Techniques, July 1977.

9. Nicolai, L. M., Fundamentals of Aircraft Design, University of Dayton, Dayton, Ohio, 1975.

10. May, F. and Widdison, C.A., STOL High-Life Design Study, Vol. 1, State-of-the-Art Review of STOL Aerodynamic Technology, AF Flight Dynamics Lab Report AFFDL-TR-71-26, Wright-Patterson AFB, Ohio, 1971.

11. Jane's All the World's Aircraft 1986-87, Jane's Publishing Co., Ltd., 1986.

12. Oates, G.C., Aerothermodynamics of Gas Turbine and Rocket Propulsion, American Institute of Aeronautics and Astronautics, Inc., 1984.

13. Mattingly, J., Heiser, W., Daley, D., <u>Aircraft Engine Design</u>, American Institute of Aeronautics and Astronautics, Inc., 1987.

INITIAL DISTRIBUTION LIST

		No. Copies
1.	Defense Technical Information Center Cameron Station Alexandria, Virginia 22304-6145	2
2.	Library, Code 0142 Naval Postgraduate School Monterey, California 93943-5002	2
3.	Professor M.F. Platzer, Code 67Pl Chairman, Department of Aeronautics Naval Postgraduate School Monterey, California 93943-5000	2
4.	LCDR Chester A. Heard USN, Code 67Ha Department of Aeronautics Naval Postgraduate School Monterey, California 93943-5000	2
5.	S. Bodapati, Code 67Bu Associate Director Navy-NASA Joint Institute of Aeronautics Department of Aeronautics Naval Postgraduate School Monterey, California 93943-5000	2
6.	R.J. Shiner Director, Man-Vehicle Systems Research Facility NASA/Ames Research Center (Mail Stop 257-1) Moffet Field, California 94035	10
7.	D.P. Bencze Associate Director Navy-NASA Joint Institute of Aeronautics Applied Aeronautics Branch NASA/Ames Research Center (Mail Stop 227-6) Moffett Field, California 94035	1
8.	MAJ P.F. Donohue USMC Marine Aviation Detachment Pacific Missile Test Center Point Mugu, California 93042	2